KRN5b regulates maize kernel row number through mediating phosphoinositol signalling

Xiaomeng Shen[1,2,3] (iD), Lei Liu[2] (iD), Thu Tran[4], Qiang Ning[2], Manfei Li[2], Liangliang Huang[1,5], Ran Zhao[2], Yunfu Li[2], Xiangyu Qing[1,5], David Jackson[2,4], Yan Bai[1,6], Weibin Song[1,5,7,8], Jinsheng Lai[1,5,7,8] (iD), Zuxin Zhang[9,*] and Haiming Zhao[1,5,7,8,*] (iD)

[1]State Key Laboratory of Maize Bio-Breeding, China Agricultural University, Beijing, China

[2]National Key Laboratory of Crop Genetics Improvement, Hubei Hongshan Laboratory, Huazhong Agricultural University, Wuhan, China

[3]The Shennong Laboratory/Grain Crops Research Institute, Henan Academy of Agricultural Sciences, Zhengzhou, China

[4]Cold Spring Harbor Laboratory, Cold Spring Harbor, New York, New York, USA

[5]National Maize Improvement Center, Department of Plant Genetics and Breeding, China Agricultural University, Beijing, China

[6]National Agricultural Technology Extension & Service Center, Beijing, China

[7]Center for Crop Functional Genomics and Molecular Breeding, China Agricultural University, Beijing, China

[8]Sanya Institute of China Agricultural University, Sanya, China

[9]Yazhouwan National Laboratory, Sanya, China

Summary

Kernel row number (KRN) is a major yield related trait for maize (*Zea mays* L.) and is also a major goal of breeders, as it can increase the number of kernels per plant. Thus, identifying new genetic factors involving in KRN formation may accelerate improving yield-related traits genetically. We herein describe a new kernel number-related gene (*KRN5b*) identified from KRN QTL *qKRN5b* and encoding an inositol polyphosphate 5-phosphatase (5PTase). KRN5b has phosphatase activity towards $PI(4,5)P_2$, $PI(3,4,5)P_3$, and $Ins(1,4,5)P_3$ *in vitro*. Knocking out *KRN5b* caused accumulation of $PI(4,5)P_2$ and $Ins(1,4,5)P_3$, resulting in disordered kernel rows and a decrease in the number of kernels and tassel branches. The introgression of the allele with higher expression abundance into different inbred lines could increase the ear weight of the inbred lines and the corresponding hybrids by 10.1%–12.2% via increasing KRN, with no adverse effects on other agronomic traits. Further analyses showed that KRN5b regulates inflorescence development through affecting the synthesis and distribution of hormones. Together, *KRN5b* contributes to spikelet pair meristem development through inositol phosphate and phosphatidylinositols, making it a selecting target for yield improvement.

Introduction

Kernel row number (KRN) is an important trait for increasing maize yield through genetic modifications. Thus, it has been a target trait in maize breeding programs. The cloning and exploitation of quantitative trait loci (QTLs) for KRN has been an effective strategy for increasing the total kernel number and yield (Hawkins *et al.*, 2013; Lopez-Reynoso and Hallauer, 1998).

The ear inflorescence development-related genes, which encode proteins that control the maize ear kernel number, influence the size and continuous differentiation of the inflorescence meristem (IM) (Liu *et al.*, 2021; Rodriguez-Leal *et al.*, 2019). For example, the CLAVATA (CLV)-WUSCHEL (WUS) feedback signalling pathway controls IM size and maintenance (Clark *et al.*, 1997; Schoof *et al.*, 2000; Wu *et al.*, 2018). In this pathway, the suppression of *WUS* gene expression ensures meristem maintenance to prevent over-proliferation and facilitate the differentiation to kernel primordia (Bommert *et al.*, 2005; Je *et al.*, 2016; Rodriguez-Leal *et al.*, 2019).

Several small molecules are important signals regulating maize inflorescence development. Phytohormones, such as auxin, cytokinin and ethylene, are naturally occurring small organic compounds involved in the regulation of meristem initiation and differentiation, which ultimately determines the number of florets and kernels (Barazesh and McSteen, 2008; Liu *et al.*, 2015; Luo *et al.*, 2022; Ning *et al.*, 2021; Zhang *et al.*, 2018). The secreted peptide CLV3 and ZmCLAVATA3/EMBRYO SURROUNDING REGION-RELATED peptide (CLE) repress *WUS* expression through different mechanisms and regulate the size of the inflorescence stem as well as the kernel number (Je *et al.*, 2016; Liu *et al.*, 2021; Rodriguez-Leal *et al.*, 2019). In maize, the spatiotemporal accumulation of the superoxide anion ($O_2 \cdot^-$), hydrogen peroxide (H_2O_2) and the hydroxyl radical can restrict the area in which *WUS* is expressed and control meristem development (Yang *et al.*, 2021). The malate content in developing inflorescences modulates reactive oxygen species (ROS) production and cell proliferation, which affects the maize ear length (Pei *et al.*, 2022). These findings have elucidated the critical role of small molecules in inflorescence development,

while also revealing promising genetic resources for increasing the maize grain yield.

Inositols (Ins) are a group of small and chemically stable polar molecules that are synthesised in cells from the glycolytic metabolite glucose 6-phosphate and then used as cytosolic solutes. Inositols and their various lipid-associated phosphate derivatives have crucial effects on signal transduction, membrane trafficking, cytoskeleton properties, cell proliferation, and permeability and transport in some bacteria, fungi and mammals (Di Paolo and De Camilli, 2006; Michell, 2008). They have biological roles in human diseases (Chakraborty, 2018; Fruman et al., 2017; Mongiorgi et al., 2016), while also controlling the accumulation and homeostasis of minerals (Duan et al., 2015; Wild et al., 2016), cell responses to environmental stimuli (Chen et al., 2008; Choi et al., 2005, 2007; Keune et al., 2013; Perera et al., 2008), and growth and development (Avila et al., 2016; Ercetin et al., 2008; Gunesekera et al., 2007; Seeds et al., 2015). However, inositol metabolism-related enzymes and their biochemical and biological effects, especially in reproductive meristems, are relatively unknown in crops.

In this study, we cloned the gene for the KRN QTL *qKRN5b* on maize chromosome 5. Specifically, *KRN5b* encodes an inositol polyphosphate 5-phosphatase (5PTase), which is responsible for hydrolyzing $PI(4,5)P_2$ and $Ins(1,4,5)P_3$ *in vivo*. We determined that *KRN5b* contributes to the regulated initiation and maintenance of reproductive axillary meristems (AMs) in the ear inflorescence, which affects the kernel number. A transcriptome sequencing (RNA-seq) analysis revealed that *KRN5b* is involved in multiple pathways related to the initiation and development of the maize spikelet pair meristem (SPM) and modulates the expression of many floret development-related and auxin synthesis-related genes. The identification and characterisation of *KRN5b* may be relevant for further clarifying the genetic basis of KRN.

Results

Map-based cloning and selected region analysis of *KRN5b*

We previously mapped the major KRN QTL *qKRN5b* within a 147.2 kb interval physically flanked by SC36031 and SC14631 on chromosome 5 using a linkage population established from two inbred lines (NX531 and SIL8) (Shen et al., 2019). Three markers from the previous study and a newly developed Kompetitive Allele-Specific PCR (KASP) marker (K13) were used to identify four recombinants (Rec1-Rec4) with overlapping genomic regions in an advanced backcross population (Figure S1). Phenotypic analysis of the progeny families derived from these recombinants indicated that the NX531 allele in the SC36031-K13 chromosomal region can significantly increase the KRN (with 0.63–0.81 additive effect, Rec3 and Rec4), resulting in an enlarged maize ear with a higher kernel number (KN) relative to the SIL8 allele (Figure S1, Tables S1 and S2). Additionally, *qKRN5b* was localised in the SC36031-K13 interval in a 32.04 kb region according to the B73_RefGen_v4 reference genome. The only annotated gene in this region, *Zm00001d013603*, encoded a phosphatidylinositol 5-phosphatase (Figure 1a). Thus, *Zm00001d013603* was designated as the candidate causal gene for *qKRN5b*, which we named *KRN5b*.

We first re-sequenced the *KRN5b* region in NX531 and SIL8 to determine the possible causal mutations for KRN variation. Comparison of the promoter region between NX531 and SIL8 detected two single nucleotide polymorphisms (SNPs) ($-523^{G/A}$

and $-1406^{C/T}$) and an 8-bp ($-828^{-/AGTGCTGC}$) insertion/deletion (In/Del) within a 3-kb region upstream of the translation start site (TSS). The coding region contained a non-synonymous SNP (G/A transition) that resulted in an alanine-to-glycine substitution at amino acid position 265 (Figure 1b).

We next analysed the diversity in the *KRN5b* region sequence among various maize inbred lines and teosinte accessions using the HapMap3 database. The interval from approximately 6 kb upstream to 4 kb downstream of *KRN5b* had a strong selection signal, with a considerable decrease in nucleotide diversity (average values: $\pi_{maize}/\pi_{teosinte} = 0.23$ and $\pi_{maize}/\pi_{landrace} = 0.28$) (Figure 1c, Bukowski et al., 2018), suggesting that *KRN5b* was selected during maize domestication and improvement.

The mRNA and protein level of *KRN5b* positively related to the kernel row number

We analysed *KRN5b* expression in immature ears of four homozygous recombinant lines derived from four heterozygous recombinants, of which Rec1 and Rec2 showed homozygous genotype with NX531 allele between the markers SC36031 and K13, while Rec3 and Rec4 were heterozygous. *KRN5b* expression did not differ between the two near-isogenic lines derived from Rec1 or Rec2. There was also no significant difference in KRN between the two lines derived from Rec1 or Rec2 (Figure S1). In contrast, $KRN5b^{NX531}$ was more highly expressed than $KRN5b^{SIL8}$ in the near-isogenic lines from Rec3 and Rec4, and the lines with higher *KRN5b* expression levels had a higher KRN (Figure 1d,e), suggesting the expression of *KRN5b* is positively related to KRN in maize.

The three sequence variations within the 3-kb region upstream of the TSS between NX531 and SIL8 may affect gene expression. Thus, we amplified a 1.7-kb segment of *KRN5b* that included the three variations from Rec3^{NX531} (i.e., P_{NX531}) and Rec3^{SIL8} (i.e., P_{SIL8}) (Figure 1f). Those segments were cloned upstream of *LUC* gene and expressed in protoplasts. The LUC activity was approximately 1.57-times greater for P_{NX531} than for P_{SIL8} ($P = 0.006$, Figure 1g), suggesting the *KRN5b* promoter activity was higher in NX531 than in SIL8. The cis-acting elements predicted using the online tool PlantCARE (Lescot et al., 2002; http://bioinformatics.psb.ugent.be/webtools/plantcare/html/) included an unnamed_2 element (CCCCGG) in the antisense strand (-523 bp), but it was not detected in P_{SIL8}, indicating the G/A SNP located 523 bp upstream of the start codon might be responsible for the differential expression of *KRN5b* between NX531 and SIL8.

KRN5b is homologous to *Arabidopsis thaliana* 5PTase proteins COTYLEDON VASCULAR PATTERN2 (CVP2), CVP2LIKE1 (CVL1) and AT3G63240 (Shen et al., 2019). The subcellular localisation analysis involving maize protoplast cells detected KRN5b − GFP in the trans-Golgi network (TGN) (Figure 1h), which is consistent with the subcellular localisation of CVP2 in *A. thaliana* (Naramoto et al., 2009). The EEP-domain of KRN5b contains two conserved 5-phosphatase domains, domains I and II (Majerus et al., 1999; Mol et al., 1995), both of which are identical to the corresponding domains in CVP2 and CVL1 (Figures 1i and S2, Carland and Nelson, 2004). Accordingly, we performed a phosphatase assay using sequences from near-isogenic maize lines. Constructs encoding the full-length sequences of KRN5b^{NX531}, KRN5b^{SIL8} or KRN5b^{mut}, which carried a mutation at amino acid position 478 in domain II, which results in phenotypic changes in *A. thaliana* (Carland and Nelson, 2004), were fused to a 6× His tag and expressed in a prokaryotic system (Figure 1j). The fusion proteins were purified to test their ability to hydrolyse a range of potential PH-binding
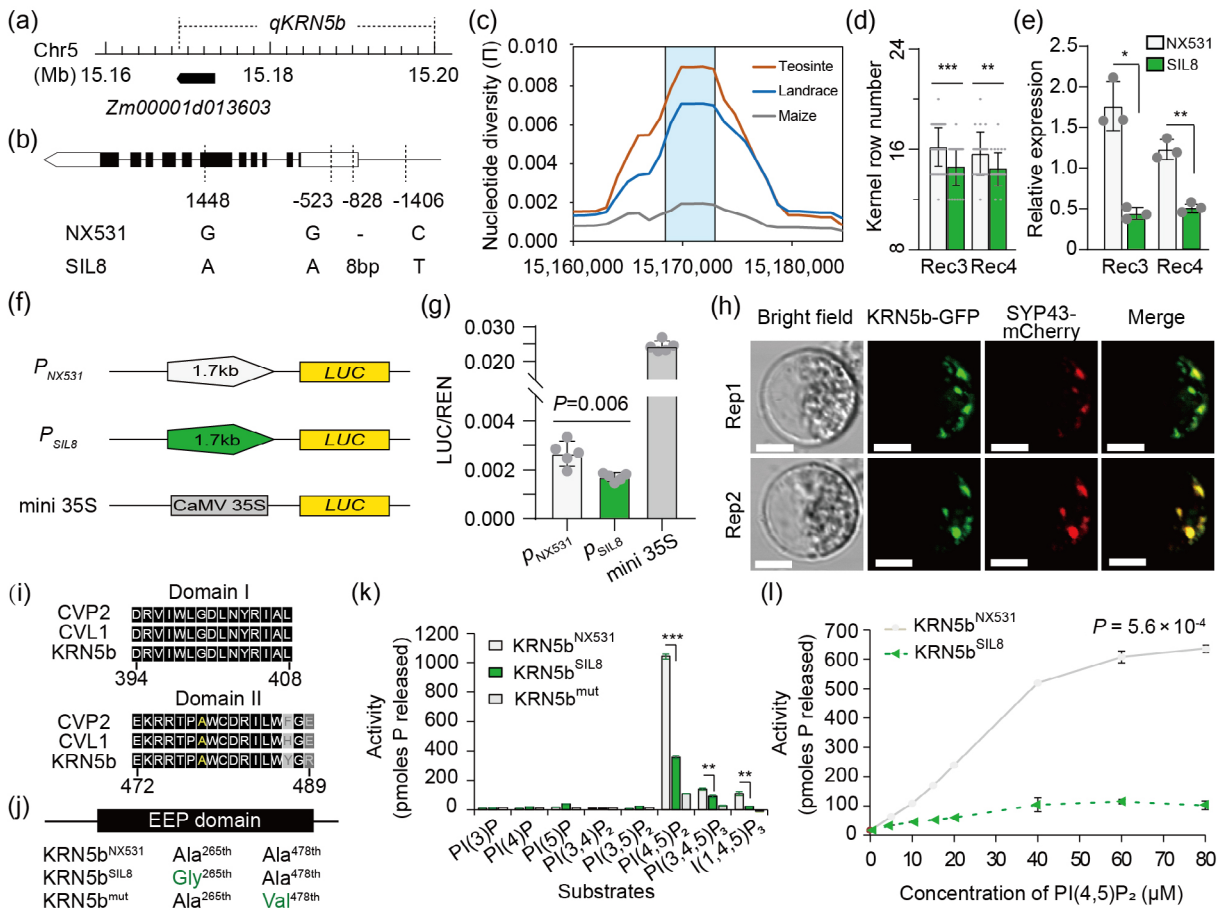
Figure 1 *KRN5b* is the candidate gene of *qKRN5b* that positively affects the kernel number. (a) Physical location of *KRN5b* on chromosome 5 of the reference genome (B73_RefGen_v4). (b) Sequence variations between NX531 and SIL8 in the *KRN5b* coding region and promoter. The black rectangle stands for the coding region, while white rectangle stands for the UTRs. (c) Nucleotide diversity (π_{maize}, $\pi_{landrace}$, and $\pi_{teosinte}$) around *KRN5b* (blue interval). (d and e) KRN (d) and the relative *KRN5b* expression levels in the developing ears (e) of the recombinant lines used for QTL mapping. Two near-isogenic lines (NIL) derived from Rec3 and Rec4 with or without introgression of *qKRN5b* from SIL8 were set for comparison for KRN and gene expression. Error bars indicate the standard deviation. * indicates a significant difference at $P < 0.05$; ** indicates a significant difference at $P < 0.01$, *** indicates a significant difference at $P < 0.001$. (f, g) Luciferase expression levels driven by P_{NX531} and P_{SIL8} (~1.7 kb), with the minimal 35S promoter used as the positive control. Data are presented as the mean (LUC/REN) $\pm$ standard deviation. The significance of any differences was assessed by Student's *t*-test. (h) Subcellular localisation of KRN5b. From left to right: bright field image, KRN5b-GFP, SYP43-mCherry, and merged fields. Scale bars = 10 μm. (i) Alignment of the conserved 5-phosphatase domains in AtCVP2, AtCVL1, and KRN5b. (j) Protein sequence variation in the endonuclease/exonuclease/phosphatase family domain (EEP domain) of KRN5b. (k) Substrates of KRN5b. Phosphatase activity was analysed using the malachite green assay, which was performed three times, each with three technical replicates. The KRN5b protein had a high affinity for $PI(4,5)P_2$, but a lower affinity for $PI(3,4,5)P_3$ and $Ins(1,4,5)P_3$. Using three phosphoinositide phosphate species as substrates, the phosphatase activity of KRN5b^{NX531} was greater than that of KRN5b^{SIL8} and KRN5b^{mut}. The significance of any differences was assessed by Student's *t*-test. **$P < 0.01$; ***$P < 0.001$. (l) Analysis of the 5-phosphatase activity of KRN5b using different concentrations of the substrate $PI(4,5)P_2$. The enzyme activity of KRN5b^{NX531} was higher than that of KRN5b^{SIL8}. Data are presented as the mean $\pm$ standard deviation. The *P*-value was estimated by Student's *t*-test.

phosphatidylinositol phosphates substrates and $Ins(1,4,5)P_3$, *in vitro*, considering that KRN5b might function similar to its ortholog CVP2 (Carland and Nelson, 2009). The phosphatase activities of KRN5b were mainly towards $PI(4,5)P_2$, and less so towards $PI(3,4,5)P_3$, and $Ins(1,4,5)P_3$. The amount of phosphate released using the KRN5b^{NX531} protein were higher than for KRN5b^{SIL8}, while KRN5b^{mut} showed no activity towards any substrate (Figure 1k). Furthermore, we compared the enzymatic activities of KRN5b^{NX531} and KRN5b^{SIL8} towards the major substrate $PI(4,5)P_2$ at a series of substrate concentrations. Saturated phosphate release was detected at 60 and 40 μM $PI(4,5)P_2$ for KRN5b^{NX531} and KRN5b^{SIL8}, respectively. Notably, the KRN5b^{NX531} activity was again higher than that of KRN5b^{SIL8} for all substrate concentrations tested

(Figure 1l). Therefore, KRN5b might function as a 5PTase that preferentially hydrolyzes $PI(4,5)P_2$. The amino acid at position 265 of KRN5b varied between KRN5b^{NX531} (alanine) and KRN5b^{SIL8} (glycine), implying the SNP affected the enzyme activity, which may contribute to the differences in KRN between the QTL parental lines.

KRN5b positively affect the KRN and kernel number of maize ear through phosphoinositide signal

To verify that KRN5b affects maize ear development, we created two *KRN5b* knockout mutants (KO1 and KO2) in the KN5585 maize inbred line genetic background using the CRISPR/Cas9 system. In both KO lines, KRN5b was terminated prematurely at its open
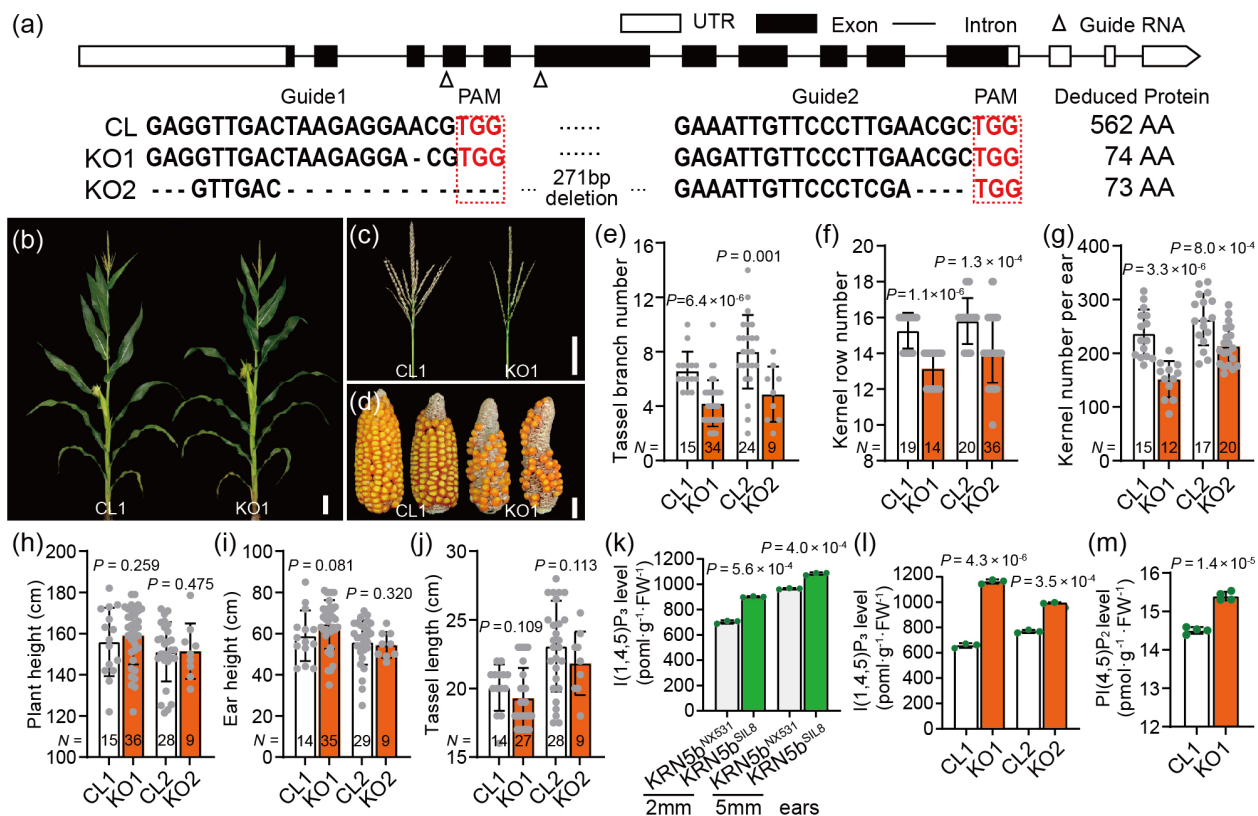
Figure 2 *KRN5b* encodes a 5PTase that affects the phosphoinositide content in immature ears as well as the maize kernel number. (a) Gene structure and guide RNA-binding sites. The TGG sequence represents the protospacer adjacent motif (PAM). (b–d) The whole plant (b), tassels (c) and ears (d) of the CRISPR/Cas9 knockout line KO1 (right) and the control line (left). Bar = 10 cm in (b and c) and 1 cm in (d). (e–g) The tassel branch number (e), kernel row number (f), and kernel number per ear (g) were reduced in KO lines. *N*, sample size. (h–j) The plant height (h), ear height (i) and tassel length (j) of KOs were equal as CLs. (k, l) Ins(1,4,5)P_3 level in the 2 and 5 mm ears of two NILs (k) and in the 5 mm ears of the KO and CL lines (l). (m) The PI(4,5)P_2 level in the 5 mm ears of the KO and CL lines. The data in (e–m) are presented as the mean ± standard deviation. The significance of any differences was assessed by Student's *t*-test.

reading frame (Figure 2a). Our phenotypic analysis revealed that the tassel branch number (TBN) and KRN was significantly lower for the KO lines than for the wild-type sibling control lines (CL1 and CL2) (Figure 2b–d), resulting in a relatively low total kernel number per ear (KN) for the KO lines, while there were no differences in plant height, ear height or tassel length (Figure 2b,c,h–j). Interestingly, the arrangement of the kernels was disordered in the KO lines and ~36% of the kernels failed to develop on the KO ear, leading to a substantial decrease in KN (Figure 2d,g).

We took the recombinant NILs derived from Rec3 (KRN5b^{NX531} and KRN5b^{SIL8}) and the KO/control lines to analyse the endogenous phosphoinositide phosphate species and Ins(1,4,5)P_3 in developing ears to confirm the 5PTase function of KRN5b. Significantly more Ins(1,4,5)P_3 accumulated in KRN5b^{SIL8} and the CRISPR/Cas9-edited lines KO1 and KO2 than in the KRN5b^{NX531} and control lines CL1 and CL2 (Figure 2k,l). Similar results were obtained for PI(4,5)P_2 (Figure 2m), indicating that Ins(1,4,5)P_3 and PI(4,5)P_2 accumulate when *KRN5b* is knocked-out. We speculate that the difference in 5PTase activity altered the production of phosphoinositide phosphate species, which may affect kernel row formation. Together, *KRN5b* positively affect KRN and might through the regulation of phosphoinositide signal.

The NX531 *KRN5b* allele increases the KRN

Two markers (SC190531 and SC22432) were developed for marker-assisted selection (MAS) and the incorporation of *KRN5b*

allele from NX531 into several inbred lines. The KRN, ear diameter (ED), and ear weight (EW) of PH4CV^{KRN5b} and Sheng68^{KRN5b} increased significantly (2.6 mm and 7.2 mm increase in ED, 2.5 row and 6.5 row increase in KRN, 7.5 g and 5.4 g in EW), while with loss of ear length (EL) in PH4CV (6.3 mm decrease) and 100 kernel weight (100 KW) in Sheng68 (3.3 g decrease) background separately (Figure 3a–e, Table S5). The KRN and EW respectively increased by 18.5% and 8.7% in the PH4CV genetic background and by 44.6% and 6.5% in the Sheng68 genetic background. In contrast, there were no changes in KRN following the introgression of the *KRN5b* allele into PH6WC or Sheng62 backgrounds (Table S5).

In an earlier study, the favourable *KNR6* allele increases EL and kernel number per row (KNPR) in two elite inbred lines (Zheng58 and H21) (Jia *et al.*, 2020). In the current study, KRN, ED, and EW increased when the *KRN5b* allele of NX531 was introduced using the same strategy (Figure 3f–k, Table S5). We therefore introgressed both *KNR6* and *KRN5b* into Zheng58, and this increased EW by 8.7% (Zheng58^{KNR6} compared with Zheng58^{ori}) and 8.0% (Zheng58$^{KNR6/KRN5b}$ compared with Zheng58$^{KNR6/−}$), respectively. The EW of Zheng58$^{KNR6/KRN5b}$ was 21.0% higher than that of the original inbred line Zheng58^{ori}, with 14.7 mm increase of EL, 2.6 increase of KNPR, and 1.7 increase of KRN. The introgression of *KNR6* in H21 increased EW by 30.8% (H21^{KNR6} compared with H21^{ori}) and the introgression of *KRN5b* increased EW by 9.2% (H21$^{KNR6/KRN5b}$ compared with H21$^{KNR6/−}$). The EW of H21$^{KNR6/KRN5b}$ was 42.1% higher than that of the original
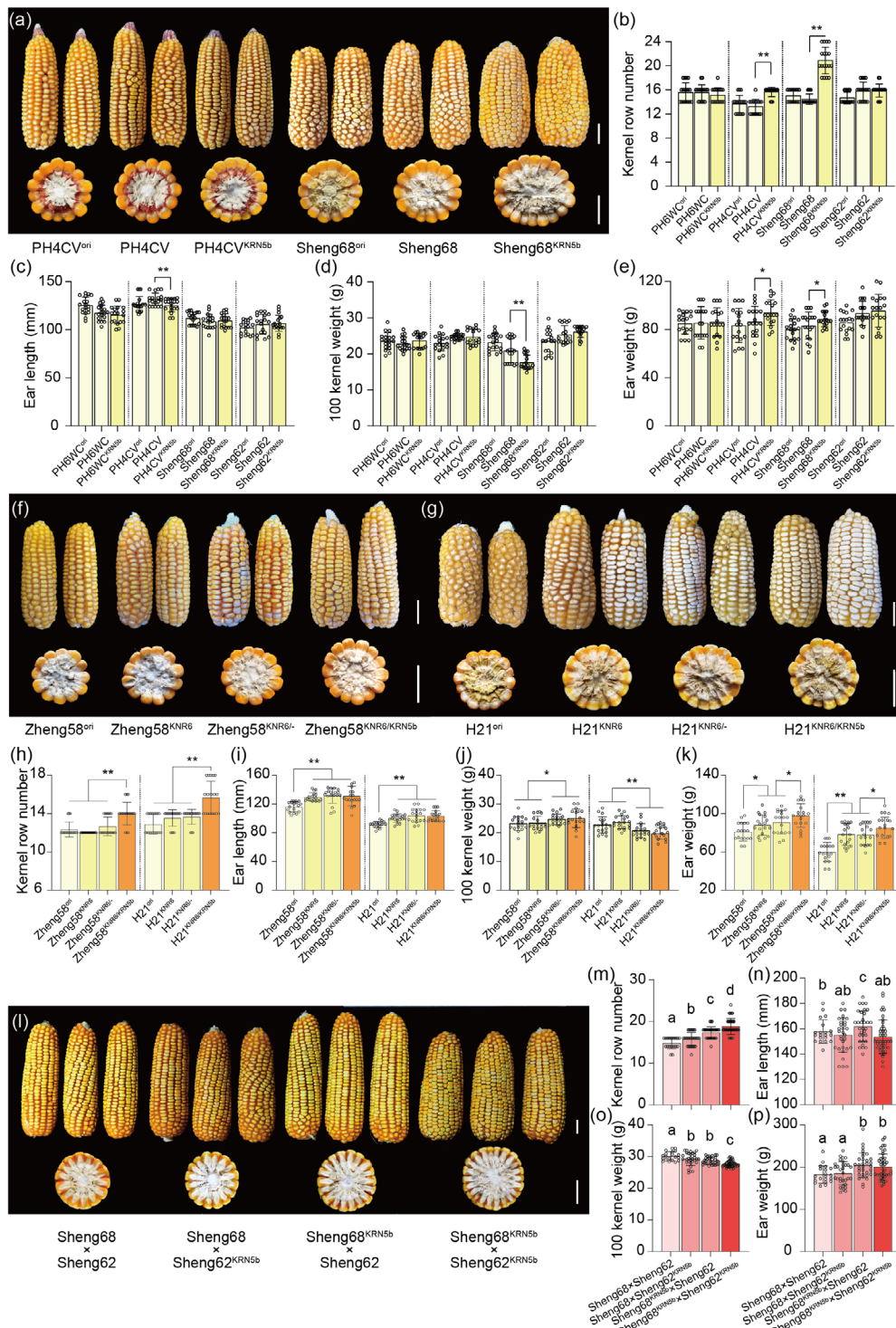
Figure 3 Marker-assisted improvement using *KRN5b* with NX531 genotype. (a–e) Effect of *KRN5b* on the maize ear traits with differing genetic backgrounds. (a) Ears of the original inbred lines PH4CV^{ori} and Sheng68^{ori}, the advanced backcrossed lines PH4CV and Sheng68 without *KRN5b*, and PH4CV^{KRN5b} and Sheng68^{KRN5b} with *KRN5b* from NX531 (homozygous genotype). (b–e) The kernel row number, ear length, 100 kernel weight, and ear weight. (f–k) Changes due to the introduction of favourable allele of *KNR6* and *KRN5b* in maize inbred lines Zheng58 and H21. (f and g) Ears of the original inbred lines Zheng58^{ori} and H21^{ori} and the genetically modified lines Zheng58^{KNR6} and H21^{KNR6}. Because of the positive effects of KNR6, lines Zheng58$^{KNR6/-}$ and H21$^{KNR6/-}$ without *KRN5b* and lines Zheng58$^{KNR6/KRN5b}$ and H21$^{KNR6/KRN5b}$ with *KRN5b* were generated. (h–k) The kernel row number, ear length, 100 kernel weight, and ear weight. (l–p) The genetic effect on maize ear of *KRN5b* in hybrid background. The *KRN5b* segment of NX531 was heterozygously and homozygously introgressed into the hybrid Sheng68 × Sheng62. (m–p) The kernel row number, ear length, 100 kernel weight, and ear weight. Scale bars = 2 cm in (a), (f), (g) and (l). The data in (b–e), (h–k) and (m–p) are presented as the mean ± standard deviation. The significance of any differences was assessed by Student's *t*-test. In (b–e) and (h–k), *$P < 0.05$; **$P < 0.01$. In (m–p), labelled means without a common letter differ $P < 0.05$. The source data are provided in Tables S5 and S6.

inbred line H21[ori], with 12.1 mm increase of EL, 4.0 increase of KNPR and 3.5 increase of KRN. EL, KNPR and 100KWs were not changed when introduced *KRN5b* of NX531 in Zheng58[KNR6] and H21[KNR6] background. These results indicate that *KRN5b* and *KNR6* might be used synergistically for the improvement of maize yield-related traits.

To verify the utility of *KRN5b* for improving the yield-related traits in maize hybrids, we used the Sheng68 and Sheng68[KRN5b] as female parent, and use Sheng62 and Sheng62[KRN5b] as male parent to produce four hybrids (Figure 3l, Table S6). The KRN of heterozygously introgressed of the NX531 *KRN5b* increased by 6.8% and 17.4% via the hybridised combination Sheng68 × Sheng62[NX531] and Sheng68[NX531] × Sheng62 separately, and 27.2% increased when homozygously introgressed via hybridised combination Sheng68[NX531] × Sheng62[NX531] (Figure 3m). The EL were not decreased when introgressed with NX531 *KRN5b* (Figure 3n), but the 100KW were 3.1% and 4.9% decreased when heterozygously introgressed and 8.2% decreased when homozygously introgressed with NX531 *KRN5b* (Figure 3o). Ultimately, the EW increased by 12.2% in Sheng68[NX531] × Sheng62 and 10.1% in Sheng68[NX531] × Sheng62[NX531] hybrids (Figure 3p). These indicates that it is necessary to pay attention to the potential dose effect of *KRN5b* and balance its impact on other traits such as 100KW.

KRN5b controls lateral organ initiation from the inflorescence meristem

Our earlier research found that *KRN5b* is highly and specifically expressed in developing ear SPMs, spikelet meristems (SMs) and floret meristems (FMs), but not in IM, suggesting that KRN5b mediates the development of lateral organ primordia from the IM (Shen *et al.*, 2019). In a normal tassel inflorescence, the IM produces primordia in a multi-rowed pattern, with the early arising primordia developing into branch meristems (BMs) and the later ones becoming SPMs. Moreover, BMs produce continuously indeterminate SPMs. In normal tassel and ear inflorescences, SPM is a type of short BM (Bortiri and Hake, 2007). One SPM forms two SMs, each of which produces two FMs (Figure 4a,c,g,i). However, the development of some tassel BM primordia was arrested in the KO lines, resulting in a decrease in the tassel branch number (TBN) (Figure 4h). In the ear and tassel inflorescences of the KO lines, some of the SPMs failed to enlarge and differentiate normally (Figure 4b, d,h,j). In the early-stage ear inflorescences, the percentage of arrested SPMs was 4-times higher in the KO lines (16%) than in the control lines (4%) (Figure 4p). The average spikelet number per branch was lower in the KO tassels (21.7 ± 3.52) than in the control tassels (26.5 ± 3.52, Figure 4q). Because of the arrested BM and SPM activities, single spikelets (SS) developed instead of paired spikelets (PS) (Figure 4f,j,m,o). Accordingly, the number of single spikelets: paired spikelets (SS:PS) was significantly higher for the KO tassels (0.50 ± 0.17 in KO1 and 0.47 ± 0.24 in KO2) than for the control tassels (0.08 ± 0.06 in CL1 and 0.14 ± 0.07 in CL2) (Figure 4r). We next counted the number of floral organs in the upper and lower tassel florets, and found a decrease in anther number in the KO tassels (Figure 4n,s,t). These results indicate that *KRN5b* is essential for initiating lateral organ primordia and determining floral organs during inflorescence development. The homeostasis of endogenous phosphoinositide phosphate species may be critical for regulating organogenesis in this process.

KRN5b-mediated phosphoinositol signalling may regulate maize inflorescence development through hormone-related genes

To clarify how KRN5b-mediated phosphoinositol signalling regulates organogenesis during inflorescence development, we performed an RNA-seq analysis in the 2 mm ear of control and knockout lines. Two hundred and seven differentially expressed genes (DEGs) were identified, of which 104 and 103 genes were respectively expressed at higher and lower levels in control than in KO, and defined as positively correlated or negatively correlated with *KRN5b* (Table S3). We subsequently performed a Gene Ontology (GO) enrichment analysis. Ten biological processes were enriched among the positively correlated genes, including responses to biosynthetic process of hormones (e.g., jasmonic acid and auxin, GO:0009695 and GO:0009851) (Figure 5a, Table S4). The expression of 6 and 5 jasmonic acid and auxin biosynthetic process genes decreased in KO ears (P_{adj} <0.05).

To identify the influence of *KRN5b* on hormone content, we measured four hormones, Abscisic Acid (ABA), Salicylic acid (SA), Indole-3-acetic acid (IAA), and jasmonic acid (JA), in 2 mm ears of knockout and control lines using liquid chromatography-mass spectrometry. The IAA and JA contents were both down-regulated in the KO ears ($P < 0.01$ (0.81- and 0.14-fold compared with the corresponding control levels, respectively), Figure 5b). Subsequently, we adopted a non-invasive micro-test technique (NMT) to detect the IAA fluxes in the normal and arrested kernel primordia in 5 mm ears (Figure 5c–g). The IAA efflux was significantly lower in the arrested spikelet primordia (Figure 5f,g), mainly due to a decrease in intracellular IAA level due to KRN5b (Figure 5b). To support this finding, we imaged the polar auxin transport protein PINFORMED1 (PIN1) in *KRN5b* mutant ear primordia. The fluorescent PIN1 immunolocalisation signals was localised in the vascular bundles and the meristems of initiated floret organs (Figure 5h–j), consistent with previous research (Gallavotti *et al.*, 2008). In *KRN5b* mutant ear primordia, the PIN1 signals were also distributed at the vascular bundles and

Figure 4 Anatomical examination of the inflorescences and spikelets. (a–d) Ear inflorescences of the CL (a, c) and KO (b, d) lines. (e, f) Enlarged scanning electron microscopy images of the ear inflorescences of the CL (e) and KO (f) lines. (g, h) Tassel inflorescences of the CL (g) and KO (h) lines. (i,j) Enlarged scanning electron microscopy images of the tassel inflorescences of the CL (g) and KO (h) lines. (k,l) Tassel central spike of the CL (k) and KO (l) plants. The central spike of the *KRN5b* knockout samples had a sparse appearance with a few spikelets and florets. (m) The pair spikelet of the CL plant and single spikelet of the KO plant. (n, o) Floral organ anatomy of the CL and KO plants (n) and diagrams representing the pair and single spikelets (o). ha, handle; pa, palea; og, outer glume; ans, anthers; ig, inner glume; le, lemma. (p–t) Percentage of arrested spikelet pair meristems in the ear inflorescence (p), average spikelet number per branch (q), single spikelet number/pair spikelet number ratio (r), anther number in the upper floret (s) and lower floret (t) for the CL and KO plants. The data in (p–t) are presented as the mean ± standard deviation. The *P*-value was estimated by Student's *t*-test. *N*, sample size. The triangle and arrowhead in (a–l) indicate normal and arrested meristems, respectively. Meristems indicated by a triangle or marked in yellow are normal spikelet meristems in (e, f) and floral meristems in (i, j), whereas meristems marked in pink are arrested spikelet meristems in (e, f) and floral meristems in (i, j). Scale bar in (a, b, e, f) = 100 μm, in (c, d, g–j) = 500 μm, in (k, l) = 2 cm, and in (m, n) = 5 mm.
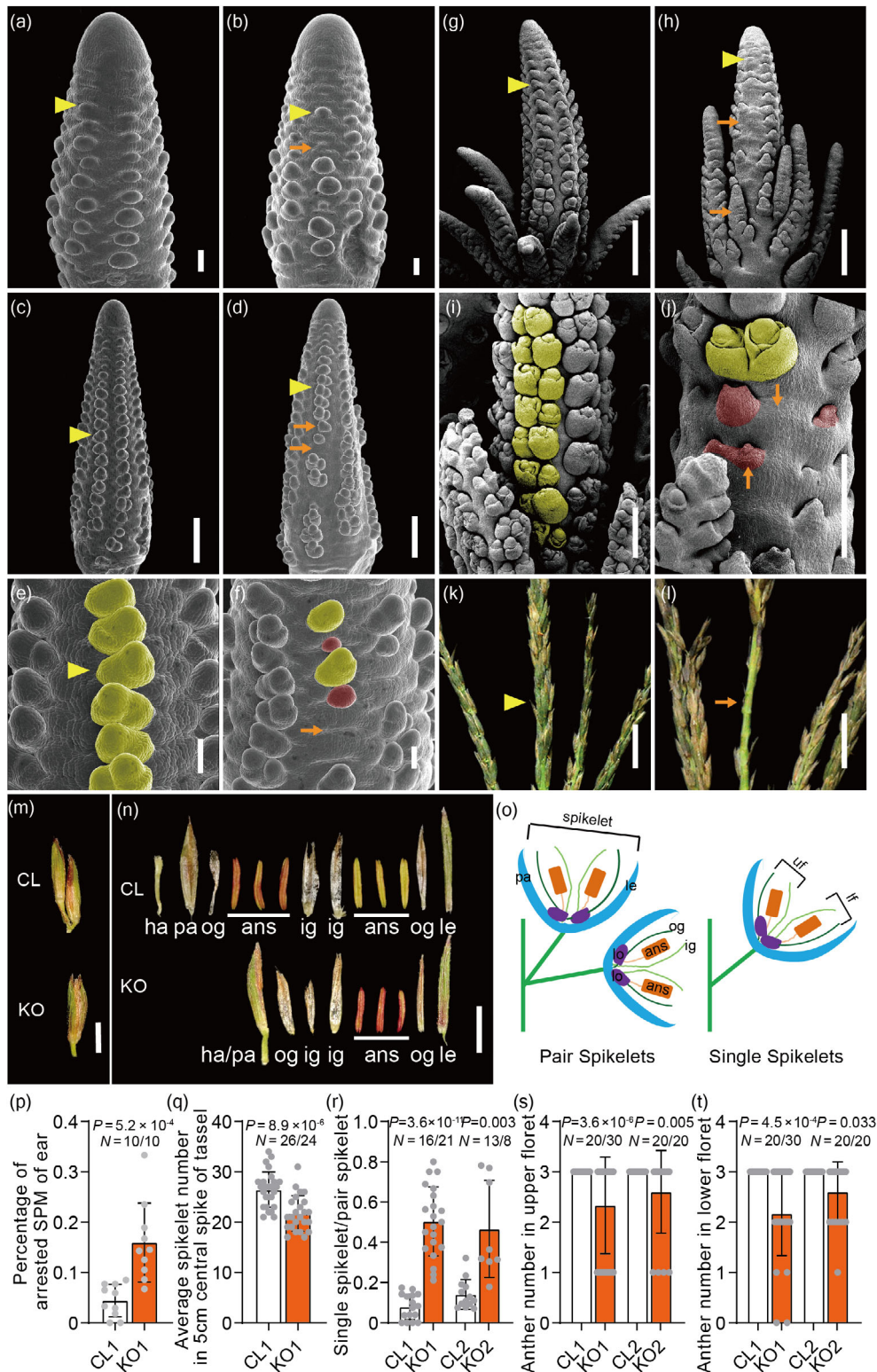
normally developed organs (Figure 5k,l) but were not observed in the arrested spikelet primordia (Figure 5k,m). Very weak and narrow regions of PIN1 signal were observed at those arrested primordia (Figure 5k,m,n). Our results indicate that *KRN5b* affected the distribution of auxin in spikelet primordia.

In summary, our results suggest that KRN5b regulates the phosphatidylinositol phosphate balance in the trans-Golgi network (TGN) by hydrolysing $PI(4,5)P_2$, contributes to the phosphatidylinositol-mediated signal transduction pathway, and controls maize inflorescence development via influence on
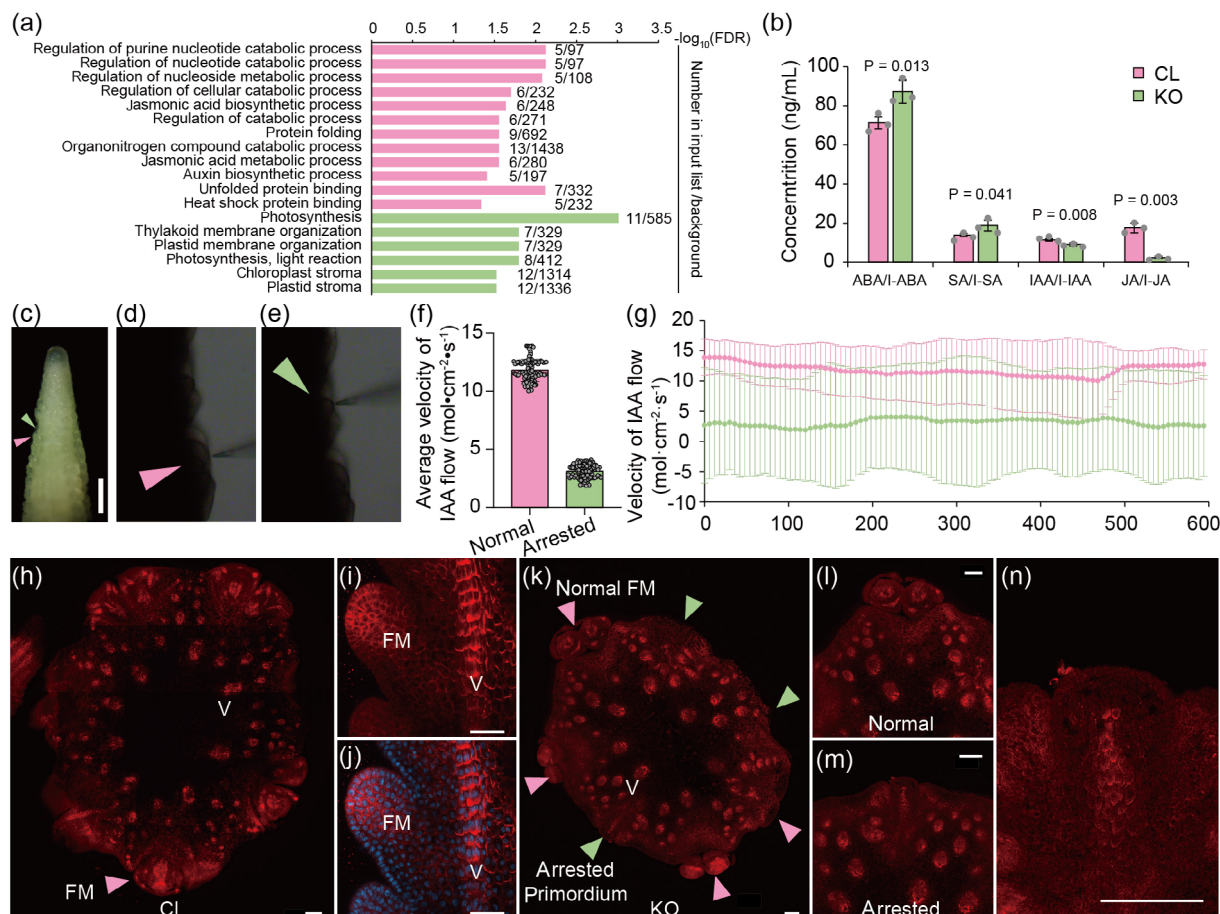
Figure 5 KRN5b regulates the maize kernel development through its influence on hormones. (a) The enriched GO terms of the differentially expressed genes between the 2 mm ear of *KRN5b* CRISPR-Cas9-edited line KO and CL. (b) Hormones contents in the 2 mm ear of the KO and L. (c–g) IAA fluxes in the 2 mm ear detected using a non-invasive micro-test technique (NMT). Pink and green arrows in (c) indicate the normal SPM (d) and arrested kernel primordium (e), respectively. Bar = 0.5 mm. (d and e) present magnified images of (c) and the location of the detectors. (f and g) Average (f) and real-time (g) IAA flow in the normal SPM (pink) and arrested kernel primordium (green). (h–n) fluorescent PIN1immunohistochemistry signals in immature ears of control (h–j) or KRN5b KO (k–n). (h) PIN1 immunolocalisation in the cross section of control ear. (i and j) PIN1 immunolocalisation (red in i and j) merged with DAPI (blue in j) in the vertical section of control ear. (k) PIN1 immunolocalisation in the cross section of KO ear. (l and m) The local features of (f) shows the normally developed FM and the arrested kernel primordium. (n) The local magnification of the (e). FM, Floret meristem; V, Vascular. Scale bar = 100 μm.

hormone content and distribution in immature ears, thereby affecting the kernel number per ear (Figure 6).

Discussion

KRN5b encodes a type I inositol polyphosphate 5-phosphatase

Phosphatidylinositol and its phosphorylated derivatives are collectively known as phosphoinositides (PIs) and phosphatidylinositol phosphates (PIPs) that are synthesised primarily in the endoplasmic reticulum in reactions catalysed by phosphoinositide kinases [PI(P)Ks] and phosphoinositide phosphatases (INPPs). The synthesised derivatives are then delivered to other membranes either by vesicular transport or via transfer proteins. In eukaryotic cells, inositol phosphates (IPs) and PIs are ubiquitously distributed in all cellular membranes as membrane lipids. The reversible phosphorylation of the inositol ring (positions 3–5) of IPs and PIPs generates diverse PI species that serve as substrates for the phospholipase-mediated production of soluble IP second

messengers (Berridge and Irvine, 1984; Strahl and Thorner, 2007) or as important regulators (Di Paolo and De Camilli, 2006; Michell, 2008).

In the phosphatidylinositol pathway, 5PTases are key enzymes that remove phosphate from PIs and IPs (position 5). The number of 5PTase genes varies among plant genomes, with 15 in *A. thaliana* and 21 in rice (Berdy *et al.*, 2001; Zhang *et al.*, 2019). Plant and mammalian 5PTases are divided into two and four major groups, respectively (Berdy *et al.*, 2001; Majerus *et al.*, 1999; Matzaris *et al.*, 1998; Minagawa *et al.*, 2001). Plant type I 5PTases, including At5PTase1 and 2, contain the inositol polyphosphate phosphatase catalytic domain that is conserved in all 5PTases. In addition to the catalytic domain, plant type II 5PTases, such as At5PTase12–14, AtFAR3, maize Brevis plant1 (BV1), and rice D50, also contain multiple N-terminal WD40 repeats (Avila *et al.*, 2016; Berdy *et al.*, 2001; Sato-Izawa *et al.*, 2012; Zhang *et al.*, 2019).

The deduced KRN5b sequence comprises 561 amino acids without an N-terminal WD40 domain. The peptide (amino
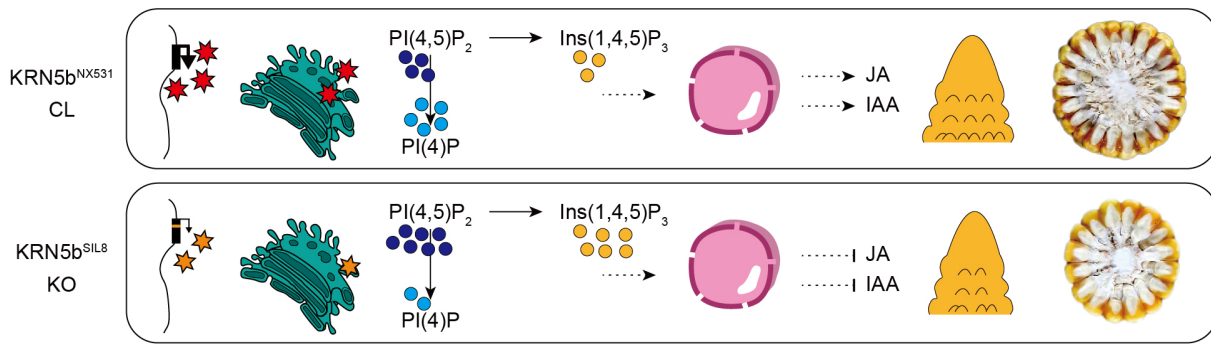
Figure 6 Model of the regulatory effects of *KRN5b* on the kernel number of maize ears. KRN5b is localised in TGN and hydrolyzes $PI(4,5)P_2$ to produce $PI(4)P$, thereby controlling the abundance of phosphatidylinositol phosphate in TGN. Additionally, KRN5b decreases the $Ins(1,4,5)P_3$ content, which is involved in phosphatidylinositol-mediated signal transduction. Moreover, *KRN5b* affects the transcription of genes related to hormone biosynthesis and response, ultimately modulating ear meristem development and the kernel number.

acids 1–519) is highly homologous to exonuclease/endonuclease/phosphatase (*E*-value = 1.06×10^{-148}), suggesting KRN5b functions as a phosphatase. According to an analysis of the domain features, KRN5b has the conserved domain I and II sequences at the catalytic region of 5PTases, indicative of the phosphatase activity of the protein (Berdy *et al.*, 2001; Majerus *et al.*, 1999). Additionally, a phylogenetic analysis showed KRN5b is clustered in the same clade as rice Os03g0663700 and *A. thaliana* CVP2 and CVL1, both of which are type I inositol polyphosphate 5-phosphatases (Carland and Nelson, 2009; Shen *et al.*, 2019). Furthermore, biochemical analyses suggest that 5PTases in the same subgroup have overlapping and unique substrate preferences. Both At5PTase1 and 2 (type I enzymes) selectively hydrolyse the water-soluble substrates $Ins(1,4,5)P_3$ and $I(1,3,4,5)P_4$ *in vitro* (Berdy *et al.*, 2001). However, in the *at5ptase1* and *at5ptase2* mutants, only $Ins(1,4,5)P_3$ accumulates (Gunesekera *et al.*, 2007), suggesting $Ins(1,4,5)P_3$ is a substrate of At5PTase1 and 2 *in vivo*. In addition, KRN5b and its homologues CVP2 and CVL1 have similar substrate preferences, with strong phosphatase activity towards $PI(4,5)P_2$, but only weak activity when the substrate is $Ins(1,4,5)P_3$ *in vitro*. Notably, $PI(4,5)P_2$ and $Ins(1,4,5)P_3$ accumulated significantly in the *KRN5b* KO lines. Considered together, these findings support the identification of KRN5b as a type I inositol polyphosphate 5-phosphatase.

KRN5b regulates inflorescence development through the phosphatidylinositol-mediated signal transduction system and affects hormone contents

There is increasing evidence that a loss of 5PTase activity leads to severely defective phenotypes with little functional redundancy, even though these enzymes share common features. For example, a lack of INPP5B, INPP5D and INPP5E leads to male sterility, haematopoietic defects, and embryonic lethality in humans and mice (Dyson *et al.*, 2012). In *A. thaliana*, the loss of functional type I enzymes, including COTYLEDON VASCULAR PATTERN 2 (CVP2) and CVP2-LIKE 1 (CVL1) that specifically catalyse reactions involving $PI(4,5)P_2$ and $PI(3,4,5)P_3$, results in an abnormal vein pattern (Carland and Nelson, 2009; Carland and Nelson, 2004; Naramoto *et al.*, 2009; Rodriguez-Villalon *et al.*, 2015). A loss-of-function mutation to FRAGILE FIBER3 (FRA3), which is a type II 5PTase with phosphatase activity towards $PI(4,5)P_2$, impairs the secondary wall synthesis in fibre cells and xylem vessels (Zhong *et al.*, 2004). At5PTase7 contributes to the salt stress response by regulating ROS production, and At5ptase11 contributes to hypocotyl growth

(Burnette *et al.*, 2003; Ercetin *et al.*, 2008; Gunesekera *et al.*, 2007; Kaye *et al.*, 2011). The recently reported suppressor of actin (SAC) domain-containing phosphatase GRAIN NUMBER AND PLANT HEIGHT1 (GH1), which specifically hydrolyzes phosphatidylinositol 4-phosphate (PI4P) and $PI(4,5)P_2$, was revealed to have pleiotropic effects on panicle morphogenesis, thereby affecting rice grain size and number (Guo *et al.*, 2020). The grain number per panicle is determined by the development of all reproductive meristems (Bommert and Whipple, 2018; Ren *et al.*, 2020), implying GH1 helps mediate rice inflorescence development.

Earlier research confirmed inositol phosphate signalling-mediated plant development is associated with auxin signalling. For example, increases in endogenous $Ins(1,4,5)P_3$ levels via the overexpression of type I 5PTases decreases the downward transport of indole-3-acetic acid in *A. thaliana* (Perera *et al.*, 2006). The *At5Ptase13* gene is reportedly modulates auxin distribution, responsive to ABA and wounding, which also antagonises PHOTOTROPIN1-mediated effects on Ca^{2+} signalling under blue light (Chen *et al.*, 2008; Lin *et al.*, 2005; Wang *et al.*, 2009; Zhong and Ye, 2004). In *5ptase12* mutant pollen grains, basal $PI(4,5)P_3$ levels and endogenous Ca^{2+} levels increase, which negatively affects precocious pollen germination along with 5Ptase13 (Wang *et al.*, 2009; Zhong and Ye, 2004). Both CVP2 and CVL1 modulate auxin distribution by regulating the intracellular cycling of PIN proteins and influence root gravitropism and vascular patterning (Carland and Nelson, 2009). A structural biology-based study demonstrated that inositol hexakisphosphate (IP_6) is a co-factor of the leucine-rich repeat domain of the auxin receptor transport response inhibitor 1 (TIR1) (Kepinski and Leyser, 2005; Tan *et al.*, 2007). Hence, there is a robust link between auxin signals and inositol polyphosphates. Finally, the double mutant *cvp2;tir1* has a more defective vein pattern than the single mutants *tir1* and *cvp2*, suggestive of a further decrease in the auxin response in the double mutant. Thus, defective 5PTase activities might disrupt auxin signalling by altering the abundance and type of inositol polyphosphate co-factors of TIR1.

As an inositol polyphosphate 5-phosphatase, KRN5b/5PTase can hydrolyses $PI(4,5)P_2$ and $Ins(1,4,5)P_3$ as substrates *in vivo* to produce $PI(4)P$ and $Ins(1,4,5)P_3$. Phosphatidylinositols and inositol polyphosphates can serve as metabolic messengers. For example, $Ins(1,4,5)P_3$, which is a second messenger in animals and higher plants, is crucial for many biological processes, including signal transduction, membrane trafficking, establishment of cell

polarity, cell wall deposition, plant responses to hormones and abiotic stresses, and plant growth and development (Heilmann, 2016). In the ear of the *KRN5b* KO line, increases in the PI(4,5)P$_2$ and Ins(1,4,5)P$_3$ contents were detected, which was in contrast to the decreases in the IAA content, IAA efflux rate, and the expression of auxin biosynthesis genes in the KO tissues. Accordingly, we infer that KRN5b regulates auxin signalling possibly by controlling inositol polyphosphate and phosphatidylinositol phosphate levels and Ca^{2+}-mediated signal transduction.

In addition to regulating auxin homoeostasis, the phospholipid signalling pathway mediates plant growth and development through several other physiological and signalling-based processes, including mechanisms affecting the intracellular distribution of phosphatidic acid-binding proteins (Ishida et al., 2007; McLoughlin and Testerink, 2013; Yao et al., 2013), responses to hyperosmotic conditions through clathrin-mediated endocytosis (Galvan-Ampudia et al., 2013) and membrane properties (e.g., via local changes in the biophysical properties of PI-enriched membrane regions) (Gerth et al., 2017). In the KO lines, the PI(4,5)P$_2$ contents increase, implying KRN5b helps to balance PI4P and PI(4,5)P$_2$ levels in cell membranes through the hydrolysis of PI(4,5)P$_2$. Hence, KRN5b affects the cell membrane physiological status, but this will need to be investigated more thoroughly in future studies.

KRN5b regulates the kernel number by controlling reproductive axillary meristem determinacy

In this study, the kernel number decreased in the *KRN5b* KO mutants because of the inactivation of the meristematic activity of partial SPMs and the failure of some SPMs to differentiate into paired SMs in the ear inflorescence. These results were consistent with the *KRN5b* expression patterns in the reproductive axillary meristem. The lack of a functional KRN5b decreases the number of normally developing tassel branches and the number of normal SPMs and SMs in tassel and ear inflorescences. Therefore, KRN5b is required for the meristematic activity of BMs and SPMs and the SM determinacy in maize inflorescences.

In the tassel inflorescence, the knocked-out of *KRN5b* leads to an obvious decrease in the spikelet number per branch and the loss of spikelets at the base of the central spike, which is similar to the phenotypes (i.e., few branches and spikelets) of the mutants with abnormal auxin biosynthesis, transport, and signalling, including *barren inflorescence2* (*bif2*) and *barren stalk2* (*ba2*) (Gallavotti et al., 2011; McSteen and Hake, 2001; Ritter et al., 2002; Tabuchi et al., 2011; Yao et al., 2019). Being treated with the auxin transport inhibitor NPA, the development SPM were also arrested (Wu and McSteen, 2007). Auxin biosynthesis and signalling in maize inflorescences have been elucidated by the systematic characterisation of key inflorescence mutants (Gallavotti, 2013; Zhang and Yuan, 2014). A shared phenotype among these auxin-related mutants is strongly repressed axillary meristems in inflorescences, resulting in inflorescences with relatively few spikelets and florets. Defective axillary meristem determinacy has also been reported for *KRN5b/5PTase* CRISPR lines, suggestive of a potential association between KRN5b/5PTase and axillary meristem determinacy in maize inflorescences.

The biotechnological applications of *KRN5b*

In the fine mapping population, the *KRN5b* showed a genetic effect to KRN of approximately 1 row. When the *KRN5b* of NX531 was introgressed into lines like Sheng68, the genetic effect increased to 3.25 rows in inbred lines, and 1.8–2.6 rows in hybrid.

However, there was no increase in KRN when the *KRN5b* of NX531 was introgressed into some genetic backgrounds such as PH6WC and Sheng62. We sequenced the CDS region and ~ 2 kb promoter region between NX531 and other inbred lines for MAS, and found multiple variations that were different from NX531 and SIL8. Therefore, we believe that the elite allele of NX531 is a rare combination, and the genetic effect of *KRN5b* varies in different backgrounds. When improving maize KRN using *KRN5b*, we recommend using the flanking molecular markers. When improving KRN of Shengrui999 (hybrid), we noticed that a decrease in the kernel number per row after introgressing the homozygous NX531 segment. In order to achieve an ideal ear shape, it is necessary to combine elite alleles from different ear traits. We have demonstrated that *KRN5b* is genetically independent to an ear length/kernel number per row QTL, known as *KNR6* (Jia et al., 2020). By utilising these QTLs together, we could effectively genetically improve the yield in different maize varieties.

Materials and methods

Plant material and field work

Two near iso-genic lines (NILs), qKRN5^{NX531} and qKRN5^{SIL8}, were developed for the fine mapping work of the KRN QTL *qKRN5b* (Shen et al., 2019). The new recombinant lines for fine mapping *qKRN5b* were screened from the advanced backcross population derived from qKRN5b^{NX531} × qKRN5b^{SIL8}. The genetic transformation receptor for producing CRISPR lines was the maize inbred line KN5585. *KRN5b* segment of NX531 were introduced into several maize inbred lines such as PH6WC, PH4CV, Sheng68, Sheng62, Zheng58^{KNR6}, and H21^{KNR6}, via backcrossed with their original inbred lines as recurrent parent for four to five generation, and selfed to homozygote at *KRN5b* combining the marker associated selection (MAS) at Wuhan (29°58′ N, 113°53′ E), Hubei, and Sanya (18°09′ N, 108°56′ E). For phenotyping the recombinant lines, CRISPR and their control lines, and those improved inbred lines with *KRN5b*, the field experiments were performed using a randomised complete block design with three replicates. For each replicate, 12 plants were grown in one row with spacing of 25 cm between plants and 60 cm between rows. At maturity, traits like plant height (PH), ear height (EH), tassel branch number (TBN) and tassel length (TL) were measured, and the ears of healthy growing plants were harvested, traits like KRN, ED, KNPR, EL, KN and EW was then measured. The mean value of all individuals with the same genotype was used as phenotype value.

During introgression of *KRN5b* in several lines with MAS, the original inbred lines were phenotyped as well, which are marked as PH4CV^{ori}, Sheng68^{ori}, Zheng58^{ori}, and so forth in Figure 5. The advance backcrossed lines with homozygote genotypes of each genetic background at *KRN5b* were set as control (marked as PH6WC, PH4CV, Zheng58$^{KNR6/−}$, etc.) to compare the genetic improvement with introgression of *KRN5b* from NX531 (marked as PH6WC^{KRN5b}, PH4CV^{KRN5b}, Zheng58$^{KNR6/KRN5b}$, etc.). Sheng68 and Sheng62 were the maternal and paternal lines of maize variety Shengrui999 (Henan, China). So we hybridised using Sheng68 and Sheng68^{KRN5b} as maternal line, while using Sheng62 and Sheng62^{KRN5b} as paternal line to produce the heterozygous and homozygous introgressed Shengrui999, to evaluate the genetic effects of *KRN5b* on hybrid.

Fine mapping of *qKRN5b*

The KRN QTL *qKRN5b* was mapped into a 147.2 kb genome region in our previous work (Shen et al., 2019). Subsequently, we

developed three In/Del markers (SC36031, SC22439, and SC44962) and one Kompetitive Allele Specific Polymorphism (KASP) marker K13 for identification of recombinants by genotyping an advanced backcross population with 2010 individuals derived from qKRN5b^{NX531} × qKRN5b^{SIL8}. In/Del marker genotypes were subjected to identify by 6% SDS-PAGE gel electrophoresis. The KASP genotyping was performed using the Bio-Rad CFX 96 and Bio-Rad T100 detection system according to the standard KASP guidelines (http://www.lgcgenomics.com). Using these markers, we identified six recombinants, which were produced from four chromosomal recombination events. All the recombinants were separately selfed to produce segregating progeny families each with 16 to 53 plants, and then these progeny families were phenotypically evaluated at Wuhan (29°58′ N, 113°53′ E), Hubei in 2018. Within each progeny family, homozygous KRN5b^{NX531}and KRN5b^{SIL8} genotypes were identified in the QTL interval by genotyping. The mean value of KRN and KN from the same genotypes was used as the phenotypic value. Significance of difference was estimated by one-way ANOVA.

Sequence analysis

The upstream sequences of *KRN5b/5PTase* from qKRN5b^{NX531} and qKRN5b^{SIL8} were amplified using gene-specific primer pairs P$_1$. The coding sequence (CDS) was amplified from the ear cDNA using primer pairs KRN5bCDS. The *cis*-acting elements in upstream sequence were predicted using the online tool PlantCare (http://bioinformatics.psb.ugent.be/webtools/plantcare/html/). Amino acid sequence of KRN5b was deduced from the CDS sequence, and was annotated with Pfam 33.1 by searching against the Pfam database (El-Gebali *et al*., 2019; http://pfam.xfam.org/). Amino acid sequences of CVP2 and CVL1 were retrieved from the Arabidopsis Information Resource (TAIR) database (https://www.arabidopsis.org/). Amino acid sequence diversity was assayed by the CLC sequence viewer 8.0 using multiple sequence alignment (MUSCLE, http://www.clcbio.com) with default parameters. The sequence identity and similarity among KRN5b, CVP2 and CVL1 were determined by BLASTP sequence alignments (https://blast.ncbi.nlm.nih.gov/).

Gene expression analysis

To analyse gene expression, 2 mm and 5 mm immature ears were collected at the ear developing stages, respectively. Total RNAs were extracted using TRIzol reagent (Ambion, Austin, TX, USA). Approximately, 1.0 μg of RNAs were reversely transcribed by the M-MLV reverse transcriptase (Life Technologies, Invitrogen, Carlsbad, CA, USA). Quantitative real-time PCR (qRT-PCR) was performed using gene specific primers q94900 in the SYBR Green qRT-PCR kit Master Mix (2×) Universal (Kapa, Boston, MA, USA) with three biological replicates, each with three technical replicates. The maize *GAPDH* gene (*Zm00001d049641*) was used as the internal control. All reactions were carried out on the CFX96 Real-time system (Bio-Rad, Hercules, CA, USA). The relative expression of the gene was calculated by the $2^{-\Delta\Delta Ct}$ method (Livaka and Schmittgen, 2001).

CRISPR-Cas9 knockout of *KRN5b* and phenotypic observation

To create mutants of *KRN5b/5PTase*, we designed guide RNAs (gRNAs) that specifically bind to target sites (GAGGTTGACTAA-GAGGAACG and GAAATTGTTCCCTTGAACGC) of *KRN5b/5PTase* using CRISPR-P 2.0 (Liu *et al*., 2017), and predicted the potential off-target sites using Cas-OFFinder in crispr rgen tools

(http://www.rgenome.net/cas-offinder/). The target sites of gRNAs are located in the 4th and 6th exon, respectively, 366 bp apart. The U6 promoter-driven gRNA CRISPR/Cas9 construct was synthesised by Sangong Biotech (Shanghai, China), and then cloned into CPB-ZmUbi-hspCas9 vector. The purified vectors were transformed into *A. tumefaciens* strain EHA101 which was used to infect the immature embryos of inbred line KN5585 through Agrobacterium-mediated transformation (Jia *et al*., 2020). We screened sequence editing events of the T$_0$ transgenic plants using gene-specific primers P949004. Those heterozygous individuals at target gene were selfed to isolate homozygous KRN5b-knockout lines (KO) and control lines (CL). KO and CL lines from one knockout event were phenotypically evaluated at Wuhan (29°58′ N, 113°53′ E) in 2019 spring and Sanya (18°09′ N, 108°56′ E) in 2019 winter, respectively. Each transgenic line was planted in a double row with three replicates, each row grew 11 plants with a spacing of 30 cm. At the silking stage, plant height (cm), ear height (cm), tassel length (cm), tassel branch number, tassel spikelet density, anther number, and number of single spikelet and pair spikelet in the central spike of tassel were measured. Mature ears are used to determine kernel row number and kernel number. All the plants for phenotyping were under the natural condition without manual pollination. Statistical significance of phenotype difference was estimated using the Student's *t*-test.

Cytological observation

Immature ear (2–5 mm) and tassel (5–10 mm) inflorescences of KO and CL lines were collected for electron microscope scanning. Inflorescence samples were fixed in a glutaraldehyde fixative solution (2.5% glutaraldehyde in 0.08 M phosphoric acid buffer) for 24 h at 4 °C, and then dehydrated through a series of ethanol from 30% to 90%. After drying, samples were coated with gold palladium by sputtering and then observed on a scanning electron microscope (SEM, JSM-6390LV, JEOL, Tokyo, Japan). The normal and arrested SPMs and SMs were counted under the scope of SMZ1270 stereomicroscope (Nikon, Tokyo, Japan).

Prokaryotic expression

Full-length coding sequences with TGA at 3′-terminal of *KRN5b* were amplified from qKRN5b^{NX531} and qKRN5b^{SIL8} using primer pairs 28aN_3603, respectively. Additionally, we synthesised a 1689 bp length mutant *KRN5b* sequence (referred to as *KRN5b^{mut}*), in which the 1436th base cytosine(C) is replaced by thymine (T), leading to a mutant protein with an alanine at the 478th amino acid that is highly conserved in the domain 2 of 5PTase family proteins, is substituted by Val. The *KRN5b^{NX531}*, *KRN5b^{SIL8}* and *KRN5b^{mut}* sequences were constructed in the pET28a vector using *Nde*I/*Xho*I restriction sites, and were then expressed as N-terminal 6 × His tag fusion proteins in *E. coli* (BL21-DE3) cell strain with 50 μg/mL kanamycin in 1 L Luria-Bertani medium. The cells were grown overnight at 37 °C, and then at 16 °C for 18 h. Protein expression was induced by addition of 0.2 mM isopropyl-β-D-thiogalactoside. After harvesting, cells were disrupted using a high pressure cell crusher and then resuspended in 20 mL lysis buffer (25 mM Tris–HCl, 150 mM NaCl, pH = 8). The insoluble fraction was removed by centrifugation at 14 000***g*** for 60 min. Proteins were purified using Ni Sepharose 6 Fast Flow column according to manufacturer's instructions (GE Healthcare, Piscataway, New Jersey, USA). Purified proteins were washed with 20 mL wash buffer (25 mM Tris–HCl, 150 mM NaCl, 15 mM imidazole, pH = 8) and were

dissolved in 1 mL elution buffer (25 mM Tris, 150 mM NaCl, 250 mM imidazole, pH = 8) for 4 times. The precipitate, supernatant, flow, wash, and elution fractions were run on SDS-polyacrylamide gel electrophoresis. The protein concentration was measured by the bicinchoninic acid (BCA) assay (Yeason, Shanghai, China).

Phosphatase activity assay

The phosphatase activity was evaluated by measuring the release of phosphorus ions (Carland and Nelson, 2009). Purified $6 \times$ His-KRN5b (1000 ng) was incubated with 1.5 mM $MgCl_2$ and 100 μM substrates (diC8 phosphoinositides, Echelon Biosciences Inc., Salt Lake City, USA, http://www.echalon-inc.com), in 50 mM Tris/HCl, pH = 7.5 (For Ins(1,4,5)P_3, $MgCl_2$ = 3 mM, pH = 6.5). A 50 μL reaction system was incubated for 45 min at 30 °C, and boiled 2 min to inactivate the enzyme. The release of phosphorus ions was monitored using a malachite green phosphatase assay kit (Echelon Biosciences Inc. Salt Lake City, USA) according to the manufacturer's protocol. Absorbance was measured at 620 nm wavelength in a SpectraMax i3x plate reader (Molecular Devices, USA). For the substrate PI(4,5)P_2, we measured a series concentration of substrates (0–80 μM) with 200 ng purified proteins, to compare the 5PTase activity among KRN5b^{NX531}, KRN5b^{SIL8} and KRN5b^{mut}.

Enzyme-linked immunosorbent assay (ELISA)

Approximately 2 mm and 5 mm the developing ears were collected from the QTL parents qKRN5b^{NX531}, qKRN5b^{SIL8} and KO lines and controls lines, respectively. More than 50 mg tissue samples were collected for each line and were grinded with a cooled mortar and pestle in liquid nitrogen. The powders were transferred into a 5 mL tube, followed by adding 10 volume of PBS (KH_2PO_4 0.24 g, Na_2HPO_4 1.44 g, NaCl 8 g, KCl 0.2 g, in 1 L ddH_2O, pH = 7.4) buffer. Enzyme-linked immunosorbent assay was performed to measure the Ins(1,4,5)P_3 level using a plant IP$_3$ ELISA kit (SbjBio, Nanjing, China) according to manufacturer's instructions. The PI(4,5)P_2 level was measured using a plant PI(4,5)P_2 Mass ELISA kit (Echelon, Salt Lake City, USA) according to its manufacturer's instructions. Absorbance was measured at 450 nm wavelength in a SpectraMax i3x plate reader with three to four biological replicates.

Dual-luciferase assay in maize protoplast

To compare the transcription activity of the promoters, we amplified a 1730 bp and a 1738 bp upstream regulatory sequence of *KRN5b/5PTase* from qKRN5b^{NX531} (P_{NX531}) and qKRN5b^{SIL8} (P_{SIL8}), respectively. The P_{NX531} and P_{SIL8} segments were constructed in the pGreenII 0800-LUC vector with *Nco*I digestion. Seedlings of maize inbred line B73 were grown in the dark at 28 °C for 5–10 days, and etiolated leaves were harvested for protoplast isolation. Maize protoplast transformation was performed using Plant Protoplast Transformation Kit (PEG-Mediated) (MKBio, Shanghai, China) according the manufacturer's instructions. Dual-luciferase detection was conducted by the Dual-Luciferase Reporter Assay System E1960 (Promega, Madison, Wisconsin, USA, https://www.promega.com) with five biological replicates.

Quantification of hormones

The 2 mm ear of CL and KO were harvested using a razor blade under the microscope. ~50 mg fresh weight of plant materials was taken for one replicate. The materials immediately frozen in liquid nitrogen were ground with pestle and extracted for 30 min at 4°C with 500 μL cold extraction buffer (isopropanol: H2O: HCl = 2:1:0.002, v/v). Fifty microliters of d_2-ABA, d_2-SA, d_2-IAA, d_2-JA was added as an internal standard for analysis. Each sample was added with 1 mL methenyl trichloride and shook (900 rpm) for 30 min at 4 °C. Then, the samples were centrifuged at 4 °C, 14 000**g** for 5 min. The 1.2 mL of lower liquid was transferred to 1.5-mL Ep tubes and evaporated by nitrogen. Each sample was resuspended in precooling methanol and mixed thoroughly. After centrifugation at 4 °C, 14 000**g** for 5 min, supernatant of each sample was filtered using a micro-spin filter tube and quantified by ultra-high-performance liquid chromatography coupled to tandem mass detection (UPLC-MS). At least three independent biological replicates of each material were tested in this assay.

IAA flux detection

We measured net fluxes of IAA by a non-invasive micro-test technique (NMT, BIO-001A, Younger USA Sci. & Tech. Corp., Amherst, MA, USA) at Xuyue Science and Technology Co., Ltd., Beijing, China. The ears of KO were harvest at 2 mm stage, with obvious mutant kernel primordia. Ears were soaked in a measuring solution (0.1 mM KCl, 0.1 mM $CaCl_2$, 0.1 mM $MgCl_2$, 0.5 mM NaCl, 0.3 mM MES and 0.2 mM Na_2SO_4, pH was adjusted to 6.0 with HCl and KOH) for 20 min, we continuously recorded the steady-state fluxes of IAAfor 10–15 min. The software of imFluxes V2.0 (YoungerUSA LLC, Amherst, MA 01002, USA), which is capable of integrating voltage signal, motion control and image capture simultaneously was used. The IAA fluxes were then calculated using the Mage Flux software developed by Xuyue (http://xuyue.net/mageflux).

Immunolocalisation of PIN1

The whole mount immunolocalisation assay were carried out following previously published protocol with minor modifications (Tran *et al.*, 2021). The ears between 0.5 and 1 cm from KO and B73 (as control) were collected and fixed in 5% acetic acid, 45% ethanol, and 10% formalin overnight, and kept in 70% ethanol. After rehydration through an ethanol series, the ears were longitudinally or transversely sectioned at 100 μm using a vibratome (Leica). The sections were incubated in cell wall digestion solution (1% Driselase, Sigma-Aldrich; 0.5% cellulase, Sigma-Aldrich; 0.75% Pectolyase, Sigma-Aldrich) for 12 min at RT. The sections were then permeabilised by incubating for 2 h in phosphate-buffered saline (PBS) buffer with 2% Tween-20, and blocked with 4% bovine serum albumin (Sigma-Aldrich) for 1 h. For the antibody reactions, the sections were incubated with an Arabidopsis PIN1 antiserum (1 : 300 dilution) (Boutte *et al.*, 2006) overnight at 4 °C. After three washes in PBS with 0.2% Tween-20, the sections were incubated overnight at 4 °C with the secondary antibody goat anti-rabbit Alexa 594 (1 : 400 dilution) (Thermo Fisher Scientific). The next day, after three washes, the sections were counterstained with DAPI (Sigma) then mounted in ProLong Gold (Thermo Fisher Scientific). Images were acquired using a Zeiss LSM 900 confocal microscope. The fluorescence signals were observed at kernel primordia that normally developed and arrested when *KRN5b* being knocked out.

Subcellular localisation

The vector construction was performed using the ClonExpress II One Step Cloning Kit (Vazyme, Nanjing, China). The CDS of *KRN5b* was amplified using gene-specific primers pSKRN5b (Table S7) containing 20 bp sequences of plant expression vector *pSuper1300::GFP*. The vector was linearised by digestion with *Pst*I and *Spe*I. The

targeted gene fragments were ligated into vectors to construct the recombinant plasmids, *pSuper*1300::KRN5b-GFP. The arabidopsis protein SYP43-mcherry was used as the TGN marker. Purified plasmid was transformed into *Agrobacterium tumefaciens* GV3101 through 30 min incubation on ice, and were submerged in liquid nitrogen for 5 min, then were incubated at 37 °C for 5 min. The transformed strains were added into 1 mL lysogeny broth (LB) liquid medium, activated at 28 °C, 160 rpm for 3–5 h and then plated on LB medium with 50 μg/mL kanamycin. A single clone of transformed *Agrobacterium tumefaciens* was used to inoculate 150 mL liquid LB medium supplemented with 50 μg/mL kanamycin and was shaking at 28 °C to an $OD600 \approx 0.5$. The bacterial liquid was re-suspended and homogenised in 5 mL of infiltration buffer (10 mM $MgCl_2$, 10 mM MES-KOH, 100 μM acetosyringone, pH = 5.6) for 2 h in the dark, and injected into tobacco cells. The infected leaves grew over night and were exposed to long daylight for 48–72 h. The fluorescent signal was visualised on a laser scanning confocal fluorescence microscope FV1200 (Olympus, Japan) using the 488-nm laser line for GFP and 588-nm laser line for RFP.

High-throughput RNA-seq analysis

Total RNAs were extracted as the method above using TRIzol reagent. Complementary DNA libraries were constructed by GENOSEQ company (Wuhan, China, www.genoseq.cn) following its pipeline including enriching mRNA with magnetic beads, randomly fragmentated the mRNA segment, synthesis of first and second strands, segment filter with AMPure XP beads, and PCR amplification, then were sequenced using the Illumina Hiseq PE150 system. Base-calling of sequence reads was performed using the Bcl2fastq software (v2.20, Illumina), and the low-quality bases were filtered by the software cutadapt (v1.13) and trimmomatic (v0.36). Experiments were repeated three times for NT and KO separately. Clean sequence reads per experiment were were mapped to Zm-B73-REFERENCE-GRAMENE-4.0. fasta using the Hisat2 software (v2.2.1, https://ccb.jhu.edu/software/hisat2/index.shtml). Gene expression values were calculated using cufflink software (v2.1.1, http://cufflinks.cbcb.umd.edu) and reported in FPKM (Fragments Per Kilobase of exon model per Million mapped fragments) units. The differential gene expression between samples was calculated using Cuffdiff software. GO term enrichment was conducted using GO term enrichment tool agriGo2 (Tian *et al.*, 2017, http://systemsbiology.cau.edu.cn/agriGOv2/). GO category FDR <0.05 was regarded as significantly enriched.

Accession numbers

Gene sequence data for this article can be found in The Maizegdb database under the following accession numbers: *Zm00001d013603* for *KRN5b*. SRA accession numbers are as follows: RNA sequence data of CL and KO ear can be found in the National Center for Biotechnology Information under accession number PRJNA1050042.

Acknowledgements

Author contributions

Declaration of interests

The authors have declared that no competing interests exist.

Data availability statement

The data that supports the findings of this study are available in the supplementary material of this article.

References

Avila, L.M., Cerrudo, D., Swanton, C. and Lukens, L. (2016) *Brevis plant1*, a putative inositol polyphosphate 5-phosphatase, is required for internode elongation in maize. *J. Exp. Bot.* **67**, 1577–1588.

Barazesh, S. and McSteen, P. (2008) Barren inflorescence1 functions in organogenesis during vegetative and inflorescence development in maize. *Genetics* **179**, 389–401.

Berdy, S.E., Kudla, J., Gruissem, W. and Gillaspy, G.E. (2001) Molecular characterization of At5PTase1, an inositol phosphatase capable of terminating inositol trisphosphate signaling. *Plant Physiol.* **126**, 801–810.

Berridge, M.J. and Irvine, R.F. (1984) Inositol trisphosphate, a novel second messenger in cellular signal transduction. *Nature* **312**, 315–318.

Bommert, P., Lunde, C., Nardmann, J., Vollbrecht, E., Running, M., Jackson, D., Hake, S. *et al.* (2005) thick tassel dwarf1 encodes a putative maize ortholog of the Arabidopsis CLAVATA1 leucine-rich repeat receptor-like kinase. *Development* **132**, 1235–1245.

Bommert, P. and Whipple, C. (2018) Grass inflorescence architecture and meristem determinacy. *Semin. Cell Dev. Biol.* **79**, 37–47.

Bortiri, E. and Hake, S. (2007) Flowering and determinacy in maize. *J. Exp. Bot.* **58**, 909–916.

Boutte, Y., Crosnier, M.T., Carraro, N., Traas, J. and Satiat-Jeunemaitre, B. (2006) The plasma membrane recycling pathway and cell polarity in plants: studies on PIN proteins. *J. Cell Sci.* **119**, 1255–1265.

Bukowski, R., Guo, X., Lu, Y., Zou, C., He, B., Rong, Z., Wang, B. *et al.* (2018) Construction of the third-generation Zea mays haplotype map. *Gigascience.* **7**, 1–12.

Burnette, R.N., Gunesekera, B.M. and Gillaspy, G.E. (2003) An Arabidopsis inositol 5-phosphatase gain-of-function alters abscisic acid signaling. *Plant Physiol.* **132**, 1011–1019.

Carland, F. and Nelson, T. (2004) Cotyledon vascular pattern2-mediated inositol (1,4,5) triphosphate signal transduction is essential for closed venation patterns of Arabidopsis foliar organs. *Plant Cell.* **16**, 1263–1275.

Carland, F. and Nelson, T. (2009) CVP2- and CVL1-mediated phosphoinositide signaling as a regulator ofthe ARF GAP SFC/VAN3 in establishment of foliar vein patterns. *Plant J.* **59**, 895–907.

Chakraborty, A. (2018) The inositol pyrophosphate pathway in health and diseases. *Biol. Rev. Camb. Philos. Soc.* **93**, 1203–1227.

Chen, X., Lin, W.H., Wang, Y., Luan, S. and Xue, H.W. (2008) An inositol polyphosphate 5-phosphatase functions in PHOTOTROPIN1 signaling in Arabidopsis by altering cytosolic Ca^{2+}. *Plant Cell* **20**, 353–366.

Choi, J.H., Williams, J., Cho, J., Falck, J.R. and Shears, S.B. (2007) Purification, sequencing, and molecular identification of a mammalian PP-InsP5 kinase that is activated when cells are exposed to hyperosmotic stress. *J. Biol. Chem.* **282**, 30763–30775.

Choi, K., Mollapour, E. and Shears, S.B. (2005) Signal transduction during environmental stress: InsP8 operates within highly restricted contexts. *Cell. Signal.* **17**, 1533–1541.

Clark, S.E., Williams, R.W. and Meyerowitz, E.M. (1997) The CLAVATA1 gene encodes a putative receptor kinase that controls shoot and floral meristem size in Arabidopsis. *Cell* **89**, 575–585.

Di Paolo, G. and De Camilli, P. (2006) Phosphoinositides in cell regulation and membrane dynamics. *Nature* **443**, 651–657.

Duan, G.L., Hu, Y., Schneider, S., McDermott, J., Chen, J., Sauer, N., Rosen, B.P. et al. (2015) Inositol transporters AtINT2 and AtINT4 regulate arsenic accumulation in Arabidopsis seeds. *Nat. Plants* **2**, 15202.

Dyson, J.M., Fedele, C.G., Davies, E.M., Becanovic, J. and Mitchell, C.A. (2012) Phosphoinositide phosphatases: just as important as the kinases. *Subcell. Biochem.* **58**, 215–279.

El-Gebali, S., Mistry, J., Bateman, A., Eddy, S.R., Luciani, A., Potter, S.C., Qureshi, M. et al. (2019) The Pfam protein families database in 2019. *Nucleic Acids Res.* **47**, D427–D432.

Ercetin, M.E., Ananieva, E.A., Safaee, N.M., Torabinejad, J., Robinson, J.Y. and Gillaspy, G.E. (2008) A phosphatidylinositol phosphate-specific myo-inositol polyphosphate 5-phosphatase required for seedling growth. *Plant Mol. Biol.* **67**, 375–388.

Fruman, D.A., Chiu, H., Hopkins, B.D., Bagrodia, S., Cantley, L.C. and Abraham, R.T. (2017) The PI3K pathway in human disease. *Cell* **170**, 605–635.

Gallavotti, A. (2013) The role of auxin in shaping shoot architecture. *J. Exp. Bot.* **64**, 2593–2608.

Gallavotti, A., Malcomber, S., Gaines, C., Stanfield, S., Whipple, C., Kellogg, E. and Schmidt, R.J. (2011) BARREN STALK FASTIGIATE1 is an AT-hook protein required for the formation of maize ears. *Plant Cell* **23**, 1756–1771.

Gallavotti, A., Yang, Y., Schmidt, R.J. and Jackson, D. (2008) The Relationship between auxin transport and maize branching. *Plant Physiol.* **147**, 1913–1923.

Galvan-Ampudia, C.S., Julkowska, M.M., Darwish, E., Gandullo, J., Korver, R.A., Brunoud, G., Haring, M.A. et al. (2013) Halotropism is a response of plant roots to avoid a saline environment. *Curr. Biol.* **23**, 2044–2050.

Gerth, K., Lin, F., Menzel, W., Krishnamoorthy, P., Stenzel, I., Heilmann, M. and Heilmann, I. (2017) Guilt by association: a phenotype-based view of the plant phosphoinositide network. *Annu. Rev. Plant Biol.* **68**, 349–374.

Gunesekera, B., Torabinejad, J., Robinson, J. and Gillaspy, G.E. (2007) Inositol polyphosphate 5-phosphatases 1 and 2 are required for regulating seedling growth. *Plant Physiol.* **143**, 1408–1417.

Guo, T., Chen, H.C., Lu, Z.Q., Diao, M., Chen, K., Dong, N.Q., Shan, J.X. et al. (2020) A SAC phosphoinositide phosphatase controls rice development via hydrolyzing PI4P and PI(4,5)P2. *Plant Physiol.* **182**, 1346–1358.

Hawkins, E., Fricker, T.E., Challinor, A.J., Ferro, C.A., Ho, C.K. and Osborne, T.M. (2013) Increasing influence of heat stress on French maize yields from the 1960s to the 2030s. *Glob. Chang. Biol.* **19**, 937–947.

Heilmann, I. (2016) Phosphoinositide signaling in plant development. *Development* **143**, 2044–2055.

Ishida, T., Hattori, S., Sano, R., Inoue, K., Shirano, Y., Hayashi, H., Shibata, D. et al. (2007) Arabidopsis TRANSPARENT TESTA GLABRA2 is directly regulated by R2R3 MYB transcription factors and is involved in regulation of GLABRA2 transcription in epidermal differentiation. *Plant Cell* **19**, 2531–2543.

Je, B.I., Gruel, J., Lee, Y.K., Bommert, P., Arevalo, E.D., Eveland, A.L., Wu, Q. et al. (2016) Signaling from maize organ primordia via FASCIATED EAR3 regulates stem cell proliferation and yield traits. *Nat. Genet.* **48**, 785–791.

Jia, H., Li, M., Li, W., Liu, L., Jian, Y., Yang, Z., Shen, X. et al. (2020) A serine/threonine protein kinase encoding gene KERNEL NUMBER PER ROW6 regulates maize grain yield. *Nat. Commun.* **11**, 988.

Kaye, Y., Golani, Y., Singer, Y., Leshem, Y., Cohen, G., Ercetin, M., Gillaspy, G. et al. (2011) Inositol polyphosphate 5-phosphatase7 regulates the production of reactive oxygen species and salt tolerance in Arabidopsis. *Plant Physiol.* **157**, 229–241.

Kepinski, S. and Leyser, O. (2005) The Arabidopsis F-box protein TIR1 is an auxin receptor. *Nature* **435**, 446–451.

Keune, W.J., Jones, D.R. and Divecha, N. (2013) PtdIns5P and Pin1 in oxidative stress signaling. *Adv. Biol. Regul.* **53**, 179–189.

Lescot, M., Déhais, P., Thijs, G., Marchal, K., Moreau, Y., Van de Peer, Y., Rouzé, P. et al. (2002) PlantCARE, a database of plant cis-acting regulatory elements and a portal to tools for in silico analysis of promoter sequences. *Nucleic Acids Res.* **30**, 325–327.

Lin, W.H., Wang, Y., Mueller-Roeber, B., Brearley, C.A., Xu, Z.H. and Xue, H.W. (2005) At5PTase13 modulates cotyledon vein development through regulating auxin homeostasis. *Plant Physiol.* **139**, 1677–1691.

Liu, H., Ding, Y., Zhou, Y., Jin, W., Xie, K. and Chen, L.-L. (2017) CRISPR-P 2.0: An improved CRISPR- Cas9 tool for genome editing in plants. *Mol. Plant* **10**, 530–532.

Liu, L., Du, Y., Shen, X., Li, M., Sun, W., Huang, J., Liu, Z. et al. (2015) KRN4 Controls Quantitative Variation in Maize Kernel Row Number. *PLoS Genet.* **11**, e1005670.

Liu, L., Gallagher, J., Arevalo, E.D., Chen, R., Skopelitis, T., Wu, Q., Bartlett, M. et al. (2021) Enhancing grain-yield-related traits by CRISPR-Cas9 promoter editing of maize CLE genes. *Nat. Plants* **7**, 287–294.

Livaka, J. and Schmittgen, T.D. (2001) Analysis of relative gene expression data using real-time quantitative PCR and the $2^{-\Delta\Delta CT}$ method. *Methods* **25**, 402–408.

Lopez-Reynoso, J.J. and Hallauer, A.R. (1998) Twenty-seven cycles of divergent mass selection for ear length in maize. *Crop Sci.* **38**, 1099–1107.

Luo, Y., Zhang, M., Liu, Y., Liu, J., Li, W., Chen, G., Peng, Y. et al. (2022) Genetic variation in YIGE1 contributes to ear length and grain yield in maize. *New Phytol.* **234**, 513–526.

Majerus, P.W., Kisseleva, M.V. and Norris, F.A. (1999) The role of phosphatases in inositol signaling reactions. *J. Biol. Chem.* **274**, 10669–10672.

Matzaris, M., O'Malley, C.J., Badger, A., Speed, C.J., Bird, P.I. and Mitchell, C.A. (1998) Distinct membrane and cytosolic forms of inositol polyphosphate 5-phosphatase II. Efficient membrane localization requires two discrete domains. *J. Biol. Chem.* **273**, 8256–8267.

McLoughlin, F. and Testerink, C. (2013) Phosphatidic acid, a versatile water-stress signal in roots. *Front. Plant Sci.* **4**, 525.

McSteen, P. and Hake, S. (2001) barren inflorescence2 regulates axillary meristem development in the maize inflorescence. *Development* **128**, 2881–2891.

Michell, R.H. (2008) Inositol derivatives: evolution and functions. *Mol. Cell. Biol.* **9**, 151–161.

Minagawa, T., Ijuin, T., Mochizuki, Y. and Takenawa, T. (2001) Identification and characterization of a sac domain-containing phosphoinositide 5-phosphatase. *J. Biol. Chem.* **276**, 22011–22015.

Mol, C.D., Kuo, C.F., Thayer, M.M., Cunningham, R.P. and Tainer, J.A. (1995) Structure and function of the multifunctional DNA-repair enzyme exonuclease III. *Nature* **374**, 381–386.

Mongiorgi, S., Finelli, C., Yang, Y.R., Clissa, C., McCubrey, J.A., Billi, A.M., Manzoli, L. et al. (2016) Inositide-dependent signaling pathways as new therapeutic targets in myelodysplastic syndromes. *Expert Opin. Ther. Targets* **20**, 677–687.

Naramoto, S., Sawa, S., Koizumi, K., Uemura, T., Ueda, T., Friml, J., Nakano, A. et al. (2009) Phosphoinositide-dependent regulation of VAN3 ARF-GAP localization and activity essential for vascular tissue continuity in plants. *Development* **136**, 1529–1538.

Ning, Q., Jian, Y., Du, Y., Li, Y., Shen, X., Jia, H., Zhao, R. et al. (2021) An ethylene biosynthesis enzyme controls quantitative variation in maize ear length and kernel yield. *Nat. Commun.* **12**, 5832.

Pei, Y., Deng, Y., Zhang, H., Zhang, Z., Liu, J., Chen, Z., Cai, D. et al. (2022) EAR APICAL DEGENERATION1 regulates maize ear development by maintaining malate supply for apical inflorescence. *Plant Cell* **34**, 2222–2241.

Perera, I.Y., Hung, C.Y., Brady, S., Muday, G.K. and Boss, W.F. (2006) A universal role for inositol 1,4,5-trisphosphate-mediated signaling in plant gravitropism. *Plant Physiol.* **140**, 746–760.

Perera, I.Y., Hung, C.Y., Moore, C.D., Stevenson-Paulik, J. and Boss, W.F. (2008) Transgenic Arabidopsis plants expressing the type 1 inositol 5-phosphatase exhibit increased drought tolerance and altered abscisic acid signaling. *Plant Cell* **20**, 2876–2893.

Ren, D., Li, Y., He, G. and Qian, Q. (2020) Multifloret spikelet improves rice yield. *New Phytol.* **225**, 2301–2306.

Ritter, M.K., Padilla, C.M. and Schmidt, R.J. (2002) The maize mutant barren stalk1 is defective in axillary meristem development. *Am. J. Bot.* **89**, 203–210.

Rodriguez-Leal, D., Xu, C., Kwon, C.T., Soyars, C., Demesa-Arevalo, E., Man, J., Liu, L. *et al.* (2019) Evolution of buffering in a genetic circuit controlling plant stem cell proliferation. *Nat. Genet.* **51**, 786–792.

Rodriguez-Villalon, A., Gujas, B., van Wijk, R., Munnik, T. and Hardtke, C.S. (2015) Primary root protophloem differentiation requires balanced phosphatidylinositol-4,5-biphosphate levels and systemically affects root branching. *Development* **142**, 1437–1446.

Sato-Izawa, K., Nakaba, S., Tamura, K., Yamagishi, Y., Nakano, Y., Nishikubo, N., Kawai, S. *et al.* (2012) DWARF50 (D50), a rice (*Oryza sativa* L.) gene encoding inositol polyphosphate 5-phosphatase, is required for proper development of intercalary meristem. *Plant Cell Environ.* **35**, 2031–2044.

Schoof, H., Lenhard, M., Haecker, A., Mayer, K.F., Jürgens, G. and Laux, T. (2000) The stem cell population of Arabidopsis shoot meristems in maintained by a regulatory loop between the CLAVATA and WUSCHEL genes. *Cell* **100**, 635–644.

Seeds, A.M., Tsui, M.M., Sunu, C., Spana, E.P. and York, J.D. (2015) Inositol phosphate kinase 2 is required for imaginal disc development in Drosophila. *Proc. Natl. Acad. Sci. USA* **112**, 15660–15665.

Shen, X., Zhao, R., Liu, L., Zhu, C., Li, M., Du, H. and Zhang, Z. (2019) Identification of a candidate gene underlying qKRN5b for kernel row number in *Zea mays* L. *Theor. Appl. Genet.* **132**, 3439–3448.

Strahl, T. and Thorner, J. (2007) Synthesis and function of membrane phosphoinositides in budding yeast, Saccharomyces cerevisiae. *Biochim. Biophys. Acta* **1771**, 353–404.

Tabuchi, H., Zhang, Y., Hattori, S., Omae, M., Shimizu-Sato, S., Oikawa, T., Qian, Q. *et al.* (2011) LAX PANICLE2 of rice encodes a novel nuclear protein and regulates the formation of axillary meristems. *Plant Cell* **23**, 3276–3287.

Tan, X., Calderon-Villalobos, L.I., Sharon, M., Zheng, C., Robinson, C.V., Estelle, M. and Zheng, N. (2007) Mechanism of auxin perception by the TIR1 ubiquitin ligase. *Nature* **446**, 640–645.

Tian, Y.L., Yan, H., You, Q., Yi, X. and Zhou, D. (2017) Wenying Xu, Zhen Su. agriGO v2.0: a GO analysis toolkit for the agricultural community. *Nucleic Acids Res.* **45**, W122–W129.

Tran, T.M., Demesa-Arevalo, E., Kitagawa, M., Garcia-Aguilar, M., Grimanelli, D. and Jackson, D. (2021) An optimized whole-mount immunofluorescence method for shoot apices. *Curr Protoc.* **1**, e101.

Wang, Y., Lin, W.H., Chen, X. and Xue, H.W. (2009) Arabidopsis 5PTase13 is involved in root gravitropism through modulating vesicle trafficking. *Cell Res.* **19**, 1191–1204.

Wild, R., Gerasimaite, R., Jung, J., Truffault, V., Pavlovic, I., Schmidt, A., Saiardi, A. *et al.* (2016) Control of eukaryotic phosphate homeostasis by inositol polyphosphate sensor domains. *Science* **352**, 986–990.

Wu, Q., Xu, F. and Jackson, D. (2018) All together now, a magical mystery tour of the maize shoot meristem. *Curr. Opin. Plant Biol.* **45**, 26–35.

Wu, X. and McSteen, P. (2007) The role of auxin transport during inflorescence development in maize (Zea mays, Poaceae). *Am. J. Bot.* **94**, 1745–1755.

Yang, R.S., Xu, F., Wang, Y.M., Zhong, W.S., Dong, L., Shi, Y.N., Tang, T.J. *et al.* (2021) Glutaredoxins regulate maize inflorescence meristem development via redox control of TGA transcriptional activity. *Nat. Plants.* **7**, 1589–1601.

Yao, H., Skirpan, A., Wardell, B., Matthes, M.S., Best, N.B., McCubbin, T., Durbak, A. *et al.* (2019) The barren stalk2 gene is required for axillary meristem development in maize. *Mol. Plant* **12**, 374–389.

Yao, H., Wang, G., Guo, L. and Wang, X. (2013) Phosphatidic acid interacts with a MYB transcription factor and regulates its nuclear localization and function in Arabidopsis. *Plant Cell* **25**, 5030–5042.

Zhang, D., Sun, W., Singh, R., Zheng, Y., Cao, Z., Li, M., Lunde, C. *et al.* (2018) GRF-interacting factor1 regulates shoot architecture and meristem determinacy in maize. *Plant Cell* **30**, 360–374.

Zhang, D. and Yuan, Z. (2014) Molecular control of grass inflorescence development. *Annu. Rev. Plant Biol.* **65**, 553–578.

Zhang, Z., Li, Y., Luo, Z., Kong, S., Zhao, Y., Zhang, C., Zhang, W. *et al.* (2019) Expansion and functional divergence of inositol polyphosphate 5-phosphatases in angiosperms. *Genesis* **10**, 393.

Zhong, R., Burk, D.H., Herbert Morrison, W.H. and Ye, Z.-H. (2004) Fragile FIBER3, an arabidopsis gene encoding a type II inositol polyphosphate 5-phosphatase, is required for secondary wall synthesis and actin organization in fiber cells. *Plant Cell* **16**, 3242–3259.

Zhong, R. and Ye, Z.H. (2004) Molecular and biochemical characterization of three WD-repeat-domain-containing inositol polyphosphate 5-phosphatases in Arabidopsis thaliana. *Plant Cell Physiol.* **45**, 1720–1728.

Supporting information

Additional supporting information may be found online in the Supporting Information section at the end of the article.

Figure S1 Fine mapping of *qKRN5b*.

Figure S2 Amino acid alignment of two KRN5b isoforms in maize and KRN5b close homologous proteins CVP2 and CVL1 in *Arabidopsis*.

Table S1 Comparison of kernel row number between near-isogenic lines.

Table S2 Comparison of kernel number per ear between near-isogenic lines.

Table S3 Differentially expressed genes between CL and KO ear.

Table S4 GO enrichment terms of differentially expressed genes between control and krn5b KO lines.

Table S5 Marker-assisted improvement in inbred lines with *KRN5b*.

Table S6 Marker-assisted improvement with *KRN5b* in hybrid backgrounds.

Table S7 List of primer sequences used in the study.